THE ROLE OF HEMODYNAMICS ON INTRALUMINAL THROMBUS ACCUMULATION AND ABDOMINAL AORTIC ANEURYSM EXPANSION: A LONGITUDINAL PATIENT SPECIFIC STUDY

By

Byron A. Zambrano

A DISSERTATION

Submitted to
Michigan State University
in partial fulfillment of the requirements
for the degree of

Mechanical Engineering - Doctor of Philosophy

2017

ABSTRACT

THE ROLE OF HEMODYNAMICS ON INTRALUMINAL THROMBUS ACCUMULATION AND ABDOMINAL AORTIC ANEURYSM EXPANSION: A LONGITUDINAL PATIENT SPECIFIC STUDY

By

Byron A. Zambrano

Abdominal aortic aneurysm (AAA), the ongoing growth of the abdominal aorta at the abdominal level is a cardiovascular disease that affects a large part of the elderly population. Among factors affecting the AAA disease, hemodynamic forces and intraluminal thrombus (ILT) are suggested to play important roles. Despite the effort made to understand these roles, much remain to be learned. This suggests a need to better understand relationships among the three factors: hemodynamics, ILT accumulation, and AAA expansion. Specially using patient-specific information of AAA patients at different times throughout the progression of the disease. Hence, this study used 59 computer tomography (CT) scans from longitudinal studies of 14 different AAA patients to analyzed the relationship between them. Various hemodynamic variables were obtained from performing computational fluid dynamics (CFD) and Lagrangian particle method on patient-specific lumen volumes of each AAA at each scan; ILT accumulation was estimated by mapping changes of ILT thickness (ΔILT) between two consecutives AAA scans, and ILT accumulation and AAA expansion rates were estimated from changes in ILT and AAA volume, respectively. Ultimately, the relationship between local values of hemodynamic parameters and ΔILT was tested on each scan of each patient using Pearson correlation coefficients. Results showed that, while low WSS was observed at regions where ILT accumulated, the rate at which ILT accumulated occurred at the same

rate as the aneurysm expansion rate (R_{sq}=0.738; $\dot{AA}_{exp} = p1 * \dot{ILT}_{acum} + p2;\ p1 = 0.87 \pm 0.203, p2 = 10440 \pm 4335$). Comparison between AAAs with and without thrombus showed that aneurysm with ILT recorded lower values of WSS and higher values of AAA expansion than those without thrombus. In fact, correlation analysis showed that among all local hemodynamic parameter tested, WSS showed to be inversely correlated to ∆ILT in approximately half of the scans from all AAA tested (52.5% of n number of scans; n=40). Vortical structures were also studied in all AAAs (with and without ILT). Results from this analysis showed that in aneurysms that developed thick ILTs, vortices consistently dissipated near zones of positive ∆ILT during the diastolic phase. In these AAAs, level of activation of platelets exposed to these vortices were estimated and results showed that none of the highest activation level recorded in any AAAs tested reached or exceeded the proposed activation threshold.

These finding suggest that while vortical structures might be important in convecting and concentrating platelets and other main coagulation species (e.g. Thrombin) on regions where positive ∆ILT is observed, these vortices might not be responsible of activating platelets. Findings also suggest, that regardless of the platelet activation pathway, low values of WSS might be promoting the formation of thrombus and submits the idea that by increasing WSS levels ILT accumulation may be prevented.

Copyright by
BYRON A. ZAMBRANO
2017

TABLE OF CONTENTS

LIST OF TABLES

LIST OF FIGURES

CHAPTER 1

Introduction

1.1 Specific aims

Abdominal aortic aneurysm (AAA) is the normal growth of the aorta at the abdominal level. This cardiovascular disease that affects a large part of the elderly population can cause death when it ruptures. In clinical practice, a maximum diameter of 5.5 cm or a growth of 1 cm/year are thresholds that assess whether a conservative (e.g. monitoring AAA growth) or a more aggressive (e.g. open surgery, endovascular repair) treatment should be performed. The selection these rupture-risk assessment variables are based on biomechanical calculations that relates variables with the probability of the wall stress to overcome the arterial wall strength [60]. Unfortunately, there have been reported cases of aneurysms rupturing under these thresholds [21] while other AAAs remained un-rupture despite their large size [58]. This highlights a pressing need to develop a more profound understanding of the different aspects influencing the progression of this disease.

Hemodynamic forces that under physiological conditions are key players of the vascular arterial remodeling [46], are being suggested to play an important role in the progression of AAAs [29,33,51,66,81]. In fact, the hemodynamic tangential force or shear has been inversely associated to the progression of other aneurysms [12]. For AAAs, however, the relationship between hemodynamics and the vascular adaptation of AAA arterial wall may not be simple in some AAAs since 75% of them are partially or fully covered by a layer of thrombus (ILT) [44].

This layer of thrombus disrupts the direct interaction between blood flow and vessel wall, potentially affecting the AAA wall strength and stress. In fact, some studies

have suggested thrombus might be promoting weakening of the arterial wall by inducing hypoxia [74,75], leading to wall thinning, cell inflammation, apoptosis of smooth muscle cells, and degradation of the extracellular matrix [49], while acting as shield, lowering and redistributing the wall stress [10,25,34,52,54,72,77]. These effects, however, are still being debated.

Despite the potential role of ILT on the progression of the AAA disease, very little is known about the mechanisms leading to its formation. Interestegly, all theories agree that hemodynamic forces are important in the formation of thrombus [13,26]. For instance, a widely accepted hypothesis suggests that thrombus forms after platelets get activated due to shear sensing and later adhere onto lumen surfaces exposed to low wall shear stress [7]. This hypothesis, however, was lately challenged, and instead a thromboactive area activating and recruiting platelets on regions of low wall shear stress has been postulated [9,43]. Nevertheless, none of these theories are being confirmed or denied.

All these studies highlight a need to analyze the complex relationship between hemodynamics, ITL and AAA growth that perhaps due to the lack of patient-specific information is still poorly understood.

The Cardiovascular Tissue and Mechanics Research Laboratory (CVTM), in collaboration with Dr. Whal Lee from Radiology department at the Seoul National University Hospital, has gathered longitudinal CT scan images of 14 patients retrospectively. Using the medical image data, the main objective is to elucidate:

1) The main hemodynamic variables that influence ILT accumulation and AAA expansion rates and their relationship between them using the longitudinal images of AAAs, with and without ILT.

2) The process of local thrombus accumulation and its association with local hemodynamic conditions. Specific local hemodynamic conditions such as wall shear stress (WSS), oscillatory shear index (OSI) and endothelium activation potential (ECAP) will be accurately estimated by using patient specific anatomic geometries and associated to local changes of thrombus thickness.
3) The shear history of platelets inside AAAs and their relationship with local thrombus accumulation. This would help to investigate the origin of thrombus and thus the role of platelets on the regional thrombus accumulation.

These objectives will be achieved by successfully completing the following aims:

*Aim 1. Construction of AAA patient specific models, calculation of global geometrical parameters and estimation of time-averaged hemodynamic parameters***.** This aim will allow us to identify the main hemodynamic differences between AAAs that developed thrombus from those that remained without significant ILT accumulation and their relationship with ILT accumulation and AAA expansion rates. Also, by observing the thrombus content at each time point (scan), we would be able to describe the thrombus accumulation process.

Aim 2. Estimation and association of regional ILT changes with local hemodynamic variables as time averaged wall shear stress (TAWSS), oscillatory shear index (OSI) and vortical structures. This will help to associate the changes of thrombus thickness with local hemodynamic environment. Using a correlation analysis, their association will be

validated with computational fluid dynamic (CFD) constructed from the retrospective data set.

Aim 3. Quantification of the shear history of platelets, and their association with local changes of ILT thickness This aim would help us to determine whether platelets are activated inside AAAs (and to confirm or deny the mechanically induced platelet activation hypothesis) and if so, the role of these platelets on the local thrombus accumulation.

By the successful completion of the presented research and with better understanding of hemodynamics and thrombus roles in the natural history of AAAs, we will be able to develop a reliable predictive model for AAAs, which are an essential tool in clinical management, risk assessment, and surgical treatment of the disease.

1.2 Background and hypothesis

Abdominal aortic aneurysms, the ongoing expansion of the aorta can cause death when it ruptures. Mechanically speaking, the rupture of an AAA occurs when the wall stresses exerted by the hemodynamic forces overcome the wall strength of the aneurysm [60]. These hemodynamic forces that consist of two components, normal and shear, have a profound impact on mechano-homeostasis of arterial and vascular remodeling [46]. Both components of these forces are also believed to play a key role in AAA pathogenesis [29,33,51,66,81].

Under normal hemodynamic shear levels (>1.5 Pa) [12], changes in wall shear stress are sensed by endothelium cells on the arterial wall modifying the surface's anti-inflammatory and anti-thrombogenic response, vasoactive tone and fibroblast activity, and extracellular remodeling [16,20,38,53,55]. Under low wall shear stress loads (<0.4 Pa), however, wall shear stress promotes atherogenic phenotype and wall degenerative

processes [53,71]. Low wall shear stress and oscillatory flow are commonly found at the distal aorta in patients with special conditions as limb amputation and spinal cord injuries, or in patients with low physical activities. These patients have been proven to have higher risk of AAA progression [27]. Interestingly, abnormal flow patterns such as low wall shear stress levels, flow separation, and formation of vortex rings are flow characteristics found even at the earliest stages of aneurysm development [8]. In addition, a lowering of hemodynamic shear stress levels were described as AAA enlarged [63]. In other types of aneurysms, for instance intracranial, a negative correlation between hemodynamic wall shear and surface displacement during expansion were found [12]. This negative direct correlation, however, may not be simple to test in AAAs since 75% of them are partially or fully covered by intraluminal thrombus (ILT) layers [44].

ILT disrupts the direct interaction between hemodynamic forces and the aneurysm wall, and potentially affecting the AAA wall strength and stress. In fact, studies that have compared AAA wall characteristics between those aneurysms with and without ILT suggested that ILT may cause hypoxia [74], wall thinning, cell inflammation, apoptosis of SMCs, and degradation of the extracellular matrix of walls covered by thick thrombus [49], thus weakening the wall and potentially lowering the wall tensile strength. It is suggested though that wall weakening in regions covered by a thick thrombus is not caused by ILT released proteases that are capable of cell degradation. It has been shown that these enzymes released by ILT at the abluminal layer are inactive [31], therefore, may not affect wall strength. Similar to its influence on wall strength, ILT is also been thought to affect wall stress. Numerical studies have found ILT to lower wall stress [10,25,34,52,54,72,77], suggesting that its presence could prevent AAA rupture. An in vivo study, however,

challenged this beneficial effect of the ILT since it found no significant pressure reduction at wall regions covered by the thrombus, suggesting no reduction in wall stress[28].

Physiologically speaking, ILT is found covering the aneurysm lumen wall, increasing its prevalence as AAA enlarges [67]. The mechanism that leads to the platelet activation and subsequent thrombus deposition are still not well understood; however, it is known that hemodynamic forces may also play an important role. Therefore, **aim 1** will focus in the analysis on the hemodynamic differences between AAAs with a thrombus accumulation from those that remained free of thrombus. Additionally, since the hemodynamic conditions are also dependent on the geometry, global values of AAA growth rate would be used to associated these three variables.

Within the last decade, the thrombus formation and accumulation in AAAs was thought to be caused by vortical structures that are commonly found inside AAAs [8] and that may activate platelets by exposing them to high shear stresses [7]. These activated platelets would later adhere at lumen walls exposed to low wall shear stress near flow recirculation zones. This theory motivated researchers to suggest potential variables to predict the accumulation of thrombus by combining the already proposed time average wall shear stress (TAWSS), Oscillatory shear index (OSI) and estimated the effect of the shear history of platelets [22]. Unfortunately, these variables have not been tested quantitatively using patient data. For this reason, **aim 2** will focus on the quantitative local association between thrombus accumulation and hemodynamic variables (as TAWSS and OSI).

Latest studies, however, are suggesting that the activation of platelets could be due to a thromboactive surface [9], conversely to what it was previously thought. This

hypothesis suggests that platelets would activated once they pass by near thromboactive wall regions and those active particles would be carried by the main flow (vortical structures) [8] to regions of persistent recirculation and relatively low TAWSS [37] where they would adhere to the wall. Unfortunately, this theory is being only tested on idealized geometries. Therefore, **aim 3** would track the shear history of platelets to determine whether platelets activates inside AAAs and thus confirm or deny the origin of the platelet accumulation.

Biochemically and biomechanically speaking, it is known that low values of wall shear stress would induce endothelium cells (ECs) dysfunction [18], with impairment of nitric oxide (NO) production [5]. NO has shown to be an effective inhibitor of platelet function [39] and the absent of it on the endothelium would lead to an initial thrombotic event [4]. However, it is still unknown whether the endothelium cell dysfunction would host or to promote a thrombus accumulation.

Once the initial ILT accumulation has taken place and the thrombus has covered lumen surface, the platelet aggregation occurs at different shear rates. At high shear rates (> 800 sec-1), von Willebrand factor (vwf) plays a critical role due to the strong bonding provided [32]. At low shear rates (< 600 sec-1), the aggregation mechanisms would be highly dependent on fibrinogen biding GPIIb/IIa [40]. This aggregation process, however, is being regulated by many antithrombotic agents that have proved to be effective and shear dependent [62]. Studies have found that fibrin surfaces degrade faster as the shear rate increases (this has been shown to be true for the range below the 500 sec^{-1} shear rate) [50]. The action of these antithrombotic agents and the fact that erythrocytes-like type of thrombus, which is usually found at the luminal layer of ILTs [1,78], is less resistance against

tPA-induced thrombolysis [47]. The antithrombotic agents would, then, regulate the platelet aggregation mechanism mediated by fibrinogen and would inhibit platelet accumulation at those shear rate ranges (~500 sec^{-1}). Therefore, aggregation and subsequently thrombus accumulation would be regulated by local hemodynamic forces.

Therefore, **aim 3** would also study the association between their activation level, hemodynamic forces and regional thrombus accumulation. This would help us to determine the role of the interaction between platelets activation and hemodynamic conditions.

CHAPTER 2

Construction of patient specific models of AAAs, calculation of global geometrical parameters, and estimation of time-averaged hemodynamic parameters

2.1 Introduction

Hemodynamic forces, intraluminal thrombus (ILT) and abdominal aortic aneurysms (AAAs) expansion are believed to interact with each other in a complex manner during the progression of this disease.

Regarding the hemodynamic forces-aneurysm expansion relationship, wall shear stress or tangential hemodynamic force is being associated with atherosclerosis in human abdominal aortas, which shares many of the mechanisms as AAAs. It has also been associated with aneurysms growth in intracranial aneurysms [12]. However, for AAA this relationship is not that simple because of the formation of thrombus.

Interestedly, the thrombus accumulation is also associated with low [22,82] and oscillatory [5] wall shear stress environment and despite this hemodynamic environment is being found in all AAAs, just 75% of them experience a thrombus deposition [44].

On the other hand, once the ILT deposition occurs, it disrupts the direct hemodynamic-vessel wall direct relationship, not just affecting the wall stress [10,25,34,52,54,72,77] and strength [49,74,75] but also promoting AAA expansion. This expansion in turn would change the main AAA geometrical features and thus modifying the hemodynamic environment.

All these previous findings have been obtained by studying the relationship between two of these three factors, indicating a close dependent among these and highlighting the importance of studying them together. The same studies have also indicated a need to analyze the main hemodynamic differences among AAAs without ILT

accumulation from those that developed thick ILTs. Hence, this chapter used longitudinal CT scans from 14 patients to investigate the relationship among hemodynamic forces, ILT accumulation and AAA expansion and the main hemodynamic differences between AAAs with and without ILT accumulation. Hemodynamic forces, represented by wall shear stress (WSS), were obtained from computational fluid dynamics; ILT accumulation was described by ILT thickness distribution changes between consecutives scans, and ILT accumulation and AAA expansion rates were estimated from changes in ILT and AAA volume. Results of this analysis showed that, while low WSS was observed at regions where ILT accumulated, the rate at which ILT accumulated occurred at the same rate as the aneurysm expansion. Comparison between AAAs with and without thrombus showed that aneurysm with ILT recorded lower values of WSS and higher values of AAA expansion than those without thrombus. Findings suggest that low WSS may promote ILT accumulation and submit the idea that by increasing WSS levels ILT accumulation may be prevented.

2.2 Methods

Sixty-two CT scans from longitudinal follow-up studies of 14 patients (Figure 2.1), taken at Seoul National University Hospital, were used for the present analysis.

	Time interval (years)					
Patients	1-2	2-3	3-4	4-5	5-6	6-7
P-1	0.50					
P-2	0.56	1.45				
P-3	1.73					
P-4	1.35	2.36				
P-5	0.48	0.50	0.49	0.48	0.52	
P-6	1.07	4.69	0.95	0.97	0.96	0.46
P-7	1.02	1.02	0.90	1.00	1.91	
P-8	1.06	1.02	1.00	0.46		
P-9	0.62	1.22	1.03	0.97		
P-10	0.27	0.46	0.82			
P-11	0.46	1.05	1.01	1.16	1.01	
P-12	2.09	0.45	0.69	0.70	0.32	
P-13	1.09	1.03	1.04			
P-14	1.23	0.46				

Table 2.1 *Time interval between two consecutive scans for 14 AAAs used*

Each patient had a set of 2 to 7 CT scans. The study had access to the time interval between scans (table 2.1). All data collection and usage were in compliance with guidelines established by the Institutional Review Board at Seoul National University Hospital and at Michigan State University.

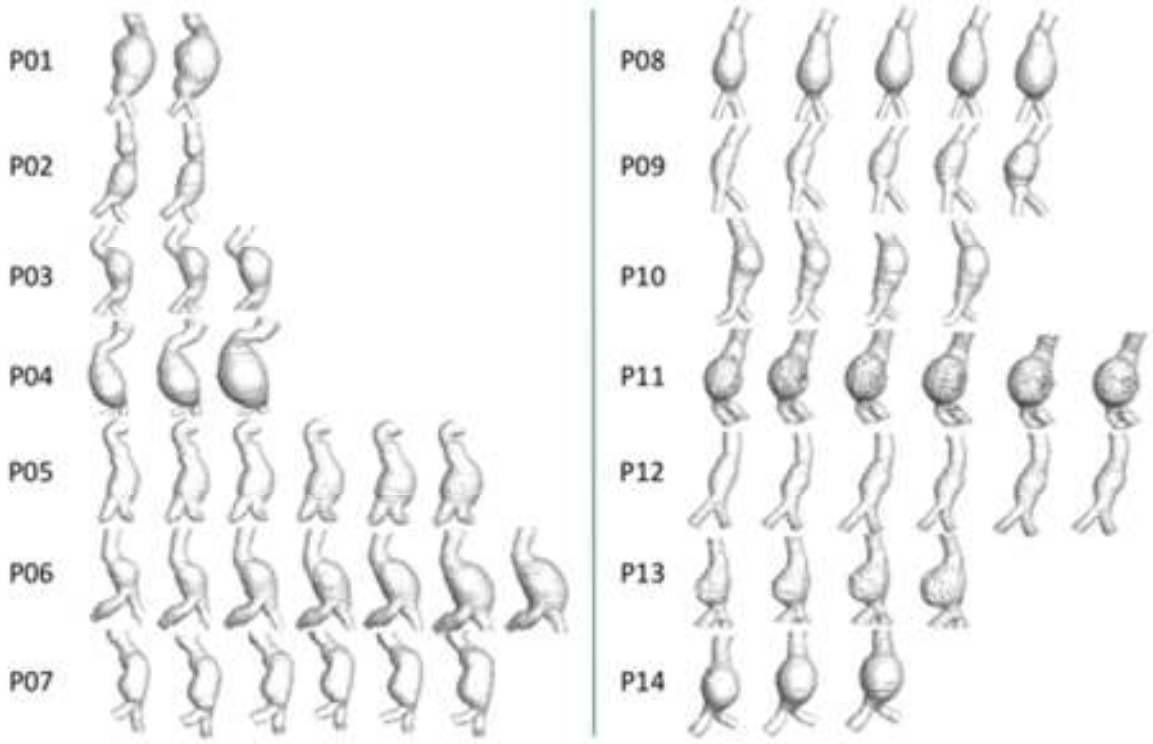

Figure 2.1 *Outer volume of each of the 14 AAAs at each time-step (scan)*

2.2.1 Volumes, diameter and cross section area calculations

Each patient's CT scan was imported to the biomedical imaging software Mimics (Materialise, Leuven, Belgium) where lumen and AAA outer volumes (Ω_l and Ω_o; respectively) were segmented, and the luminal and outer wall surfaces Γ_l and Γ_o were extracted. Once extracted, lumen and AAA volumes were calculated between orthogonal planes to the centerline between the lower renal branch and the iliac bifurcation levels. The ILT volume was then estimated by subtracting the AAA outer volume (Ω_o) minus Lumen volume (Ω_l).

For the maximum diameter calculation, the method of inscribed spheres [19], which consist of calculating diameters of maximally inscribed spheres along the

centerline, was used. Therefore, the largest value of the diameter along the centerline was defined as the maximum diameter.

To calculate AAA's outer and lumen cross-section areas at the location of maximum diameter, an orthogonal plane to the centerline at the location of the maximum diameter was first generated [35]. The intersection between the orthogonal plane, the AAA's outer wall and lumen wall surface were used to delineate cross section areas. After delineating the cross-section contour, the cross-section areas for AAA and lumen were generated and calculated.

2.2.2 Growth measurements

AAA expansion and ILT accumulation rates were estimated based on the changes in AAA and ILT volumes between two consecutives scans as follows:

$$\frac{\Delta\Omega}{\Delta t} = \frac{\Omega^{i+1} - \Omega^{i}}{t^{i+1} - t^{i}} \tag{2.1}$$

2.2.3 ILT morphology

Characterization of the thrombus content on each AAA at each time-point was performed by using lumen and AAA outer surfaces (Γ_l and Γ_o; respectively). Specifically, ILT thickness at a given point was defined as the minimum distance between these two surfaces (Figure 2.2).

Since it was challenging to delineate the boundaries between the aneurysmal wall and the thrombus layer using CT scans, the minimum distance approximation method would include the aneurysmal wall thickness. Previous studies have estimated the AAA wall thickness to be between 0.23 mm and 4.23 mm [24,59,72]. Therefore, a constant value

of 3.5 mm was subtracted to the initial calculation. Therefore, for given $\boldsymbol{x_1} \in \Gamma_l$ and $\boldsymbol{x_2} \in \Gamma_o$, ILT thickness is defined as:

$$ILT^i(\boldsymbol{x_1}) = \min\|(\boldsymbol{x_2} - \boldsymbol{x_1})\| - 3.5\text{mm}, \qquad \forall\, \boldsymbol{x_2} \in \Gamma_o, \tag{2.2}$$

whereas if $ILT^i(\boldsymbol{x_1})$ is positive, otherwise $ILT^i(\boldsymbol{x_1})$ is zero.

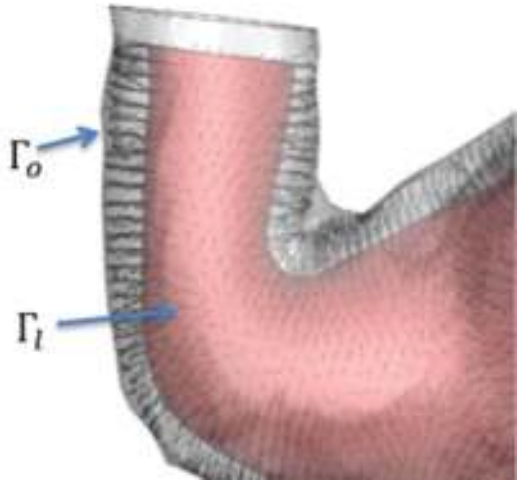

Figure 2.2 *AAA outer and lumen surfaces depicting the minimum distance approximation method between these two surfaces*

2.2.4 AAA classification accordantly to thrombus content

To study the relationship between hemodynamic forces, AAA growth and ILT accumulation, each scan of each patient was classified as one with or without an ILT content using the wall fraction of area covered by ILT criteria. The fraction was calculated by dividing the measure of the AAA wall area covered by ILT over the surface measurement of the AAA wall. A surface fraction threshold of 0.2 was assumed and used as a threshold to classify AAAs in two groups: “AAAs with ILT” and “AAAs without ILT”. Classifying scans independently rather than patients helped to increase the accuracy of our observations since ILT can be accumulated at any time during the surveillance period.

2.2.5 Computational fluid dynamic (CFD) analysis

Hemodynamic variables were estimated by performing computational fluid dynamics (CFD) simulations on each AAA's lumen volume (Ω_l) at each time-point (or scan). For each computational domain, renal branches were trimmed and model were truncated above the renal level and after iliac bifurcation to define inlet and outlets boundaries; respectively. Since a fully developed flow assumption was used at the inlet and outlet boundaries, the specific location of these truncations for the CFD analysis changed from patient to patient.

Additionally, extended boundaries were created at the inlet and outlets of the flow by approximately three times the inflow diameter in order to avoid numerical instabilities (Figure 2.3) [6]. The estimation of the extension length was done using the relationship suggested by Wood and colleagues [79].

All lumen volumes of all patients were used except patient 4. The CT image resolution required to obtain an accurate estimation of the WSS values for patient 4 was not optimal; and, therefore, this patient was excluded just from the CFD analysis.

Once the computational domain was defined, models were meshed using ICEM (ANSYS Inc, Lebanon, NH, USA). A sensitivity analysis was performed by using 4 different element sizes (0.95, 0.8, 0.6, and 0.55 mm) and by testing our variables of interest (i.e., WSS). From this preliminary CFD analysis, a mesh of an element size of 0.6 mm was found to be optimal for this analysis. This edge length resulted in a mesh size that ranged between approximately 5-8 millions of elements. The element size and computational size domain obtained from this analysis are similar to what others have reported for similar CFD analysis [5,14,22].

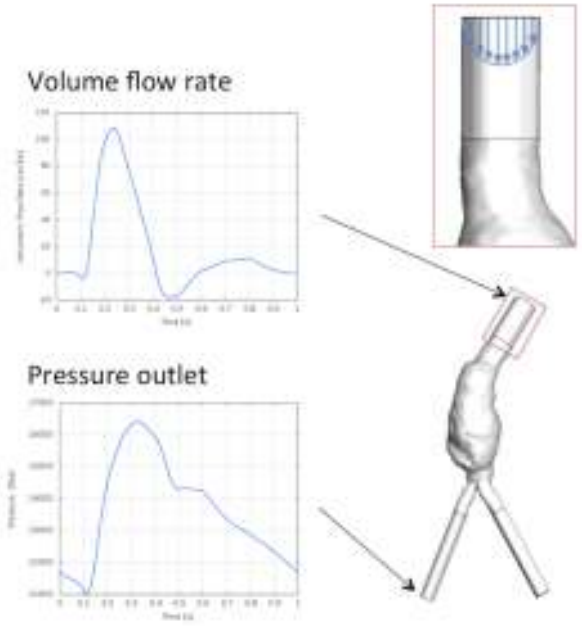

Figure 2.3 *Volume flow rate and pressure outlet waves imposed at the inlet and outlet, respectively. This figure also shows the inlet and outlet extension made to the inlet and outlet boundaries in order to avoid numerical instabilities*

Once defined the computational domain Ω_l, continuity and the incompressible Navier-Stoke equations were solved for velocity ($\boldsymbol{v}$) and pressure (p) (Eq. 2.3 and 2.4).

$$\nabla \cdot \boldsymbol{v} = 0 \ , \tag{2.3}$$

$$\rho(\frac{\partial \boldsymbol{v}}{\partial t} + \boldsymbol{v} \cdot \nabla \boldsymbol{v}) = \nabla \cdot \boldsymbol{\sigma} + \boldsymbol{f} \ , \tag{2.4}$$

where ρ, $\boldsymbol{v}$, $\boldsymbol{\sigma}$ and $\boldsymbol{f}$ represent the blood density, the velocity vector, the stress tensor and the external or body force, respectively. For these simulations, the external and body force were assumed to be zero. The stress tensor can be decomposed into: hydrostatic (p) and deviatoric stress ($\boldsymbol{\tau}$)

$$\boldsymbol{\sigma} = -p\boldsymbol{I} + \boldsymbol{\tau}, \tag{2.5}$$

$$\boldsymbol{\tau} = \mu \boldsymbol{D}, \tag{2.6}$$

where the deviatoric stress can be represented as a function of the shear rate tensor ($\boldsymbol{D}$) and the viscosity (μ). The disaggregation of red blood cells (RBCs) due to shear stresses

makes blood to be considered a non-Newtonian fluid with high shear-thinning. This shear-thinning behavior has an impact on the flow structure, including in the fluid circulation near the surface [37] and it was captured in the present study by using the Carreau-Yasuda model (Figure 2.4) [36]. This is mathematical defined as:

$$\frac{\mu-\mu_\infty}{\mu_o-\mu_\infty} = [1 + (\lambda\dot{\gamma})^a]^{\frac{n-1}{a}}, \tag{2.7}$$

$$\dot{\gamma} = \sqrt{2\boldsymbol{D}:\boldsymbol{D}}\ , \tag{2.8}$$

where $\dot{\gamma}, \boldsymbol{D}, \mu_o\ , \mu_\infty, \lambda, n, a$ represent the scalar shear stress, symmetric part of the velocity gradient, lower and higher spectrum of viscosity, the power index and the Yasuda exponent, respectively.

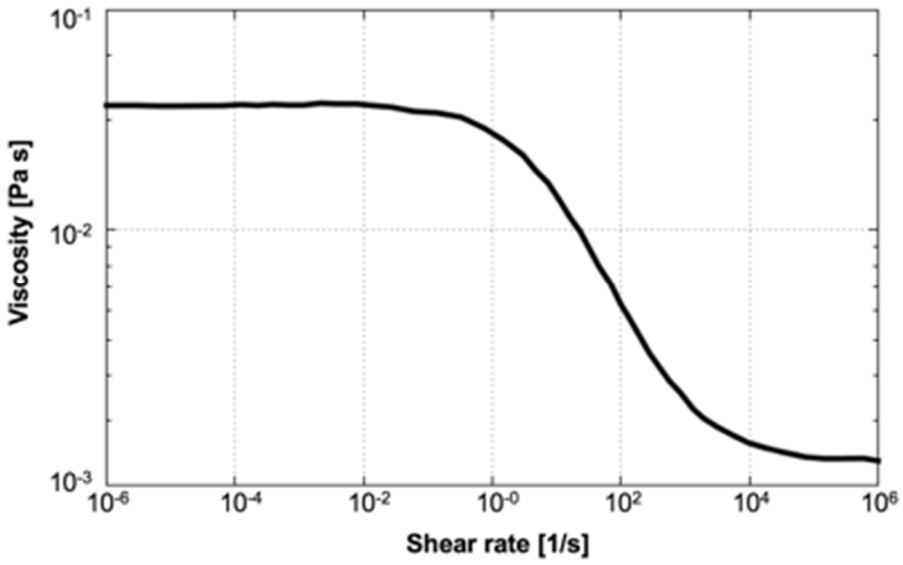

Figure 2.4 *Viscosity vs shear rate predicted by using the Carreau-Yasuda viscosity model used to capture the non-Newtonian behavior*

Hemodynamic simulations using FLUENT (ANSYS Inc, Lebanon, NH, USA) were performed on each lumen model under the assumption of laminar incompressible flow (ρ=1060 Kg/m3) with rigid walls. Idealistic time-dependent volume flow rate and pressure

waves were imposed at the inlet and outlets based on data presented by Olufsen and colleagues [57] (Figure 2.3).

A time step of 0.001s (1000 time step per cardiac cycle) was chosen and the flow field was saved every 5 time steps (200 time steps per cardiac cycle). In order to minimize the error due to the initial condition, the first two cardiac cycles were discarded from the analysis and the third cardiac cycle was averaged to obtain a time-average wall shear stress (TAWSS) values. This variable is mathematically defined as follows:

$$\boldsymbol{t} = \boldsymbol{\sigma n}_{\Gamma_l} \tag{2.9}$$

$$\boldsymbol{wss} = \boldsymbol{t} - \left(\boldsymbol{t} \cdot \boldsymbol{n}_{\Gamma_i}\right)\boldsymbol{n}_{\Gamma_l} \tag{2.10}$$

$$TAWSS = \frac{1}{(T_2 - T_1)} \int_{T1}^{T2} \|\boldsymbol{wss}\| \, dt \tag{2.11}$$

2.2.6 Relations between measurements and statistical analysis

Statistical analyses were performed using the Matlab software (Mathwork, Natick, USA). A linear regression was used to examine the relationship between the ILT accumulation rate and the AAA expansion rate on AAA's CT scans classified as with an ILT accumulation. Additionally, the relationship between the maximum equivalent diameter and maximum ILT thickness at the region of maximum diameter was investigated using Pearson's correlation coefficient for all patients.

2.3 Results

2.3.1 Classification according to the AAA wall area covered by ILT

In order to understand hemodynamic differences between AAAs with an ILT accumulation from those that did not show ILT, each patient was analyzed according to the area covered by thrombus. Results from this analysis showed that 5 patients presented a

significant ILT accumulation from the beginning of the surveillance study (P4, P10, P11, P13, P14), 4 patients showed an ILT buildup while AAAs were under surveillance (P5, P6, P8, and P9), and 5 patients were found not to show any significant ILT accumulation (P1-P3, P7, and P12; Figure 2.5 a). The ILT thickness distributions of patients at their last scans are shown in Figure 2.5 b.

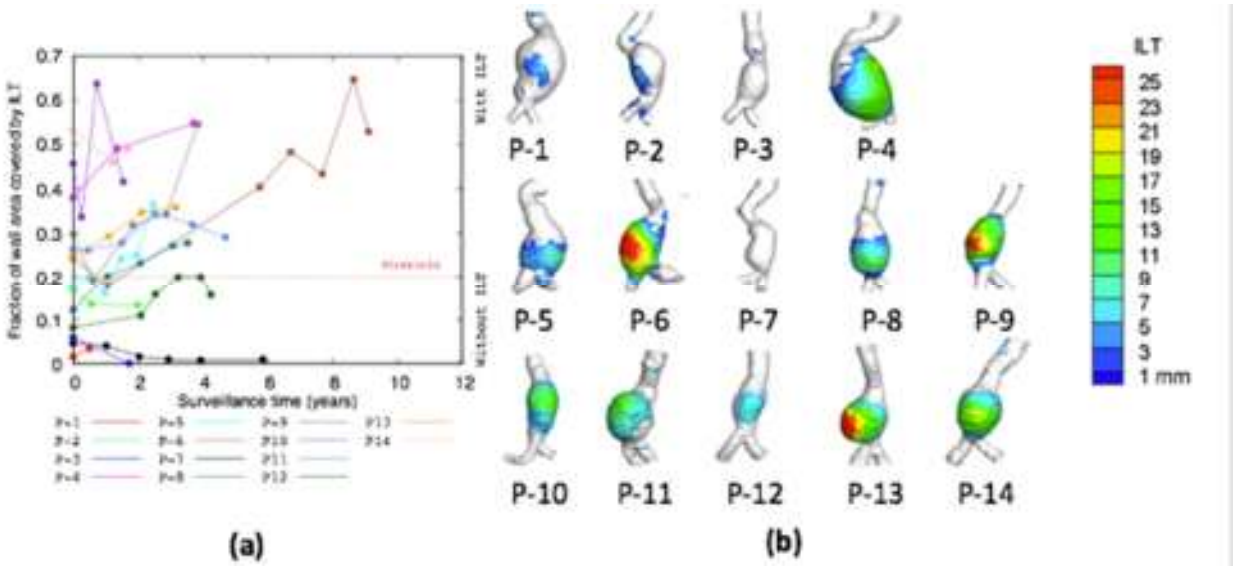

Figure 2.5 *(a) Fraction of AAA wall area covered by ILT showing classification between AAAs with and without ILT according to the 0.2 threshold (---) (b) The ILT thickness distribution of all AAAs at their respective last scan for each patient.*

2.3.2 ILT accumulation process

In AAAs that showed an ILT buildup, observed spatial distribution of the ILT thickness through time showed that all followed a common development pattern (Figure 2.6). Specifically, all ILTs began as a localized buildup at the region of maximum diameter. From this region, ILTs spread to the surrounding areas at the same time as an increase in ILT thickness was observed on areas previously covered by ILT. This process occurred gradually as the aneurysm expanded. Sequential 3-D images (Figure 2.6a) and circumferentially averaged values of ILT thickness plotted in the longitudinal direction

(Figure 2.6b) demonstrate this ILT growth pattern in patients P-8 and P-9 as an example of the common pattern found in all patients with an ILT buildup. Note that in both patients, the location where the thrombus was the thickest varied throughout the scans but was located within regions of maximum diameter.

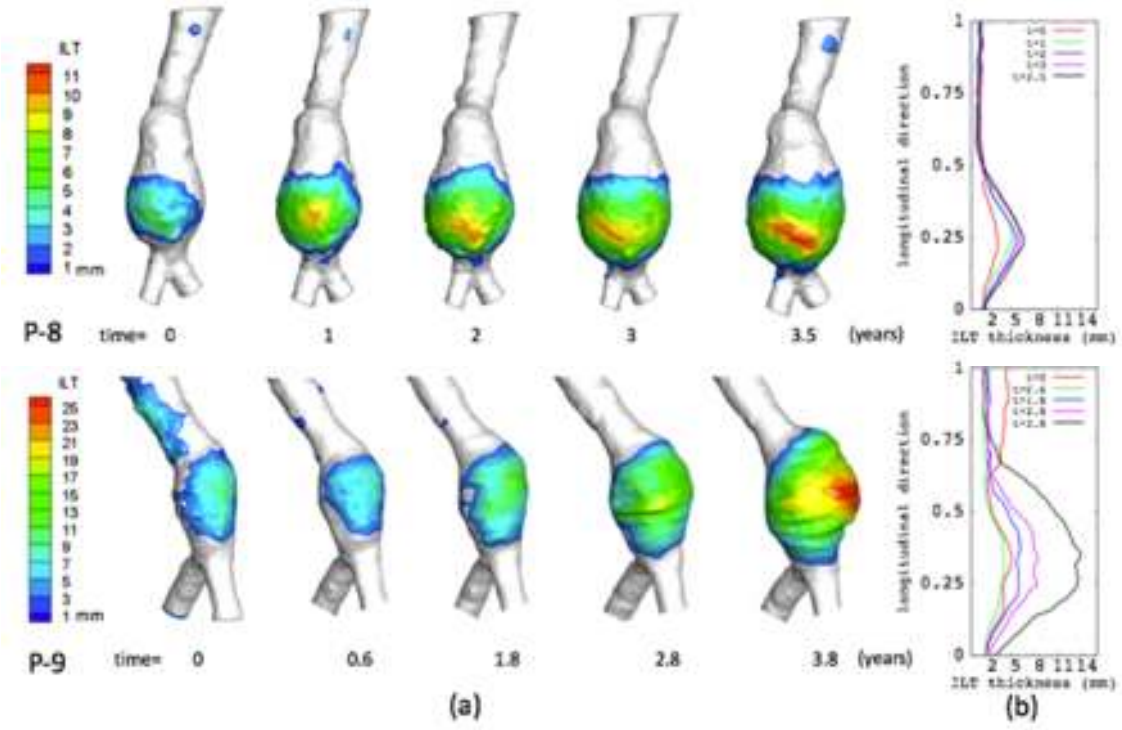

Figure 2.6 *The ILT accumulation process using: (a) Spatial distribution of ILT thickness for patients P-8, and P-9 at all their scans, and (b) the circumferentially averaged values of ILT along centerline.*

A positive correlation coefficient between maximum ILT thickness and maximum diameter was found for all patients with ILT, which agrees with the above described accumulation process ($r=0.681$, $P<.001$).

2.3.3. CFD analysis

2.3.3.1 Blood flow pattern

Results from CFD analysis performed on all aneurysms showed some similarities and differences in the blood flood pattern between AAA's that showed an ILT deposition from those that did not develop it. While recirculation zones inside the sac region that formed after peak systolic and in some cases remaining through the cardiac cycle was commonly observed among them, the magnitude of the velocity of these recirculation zones near the lumen wall showed to be lower in AAAs that developed ILT from those that remained without a significant accumulation.

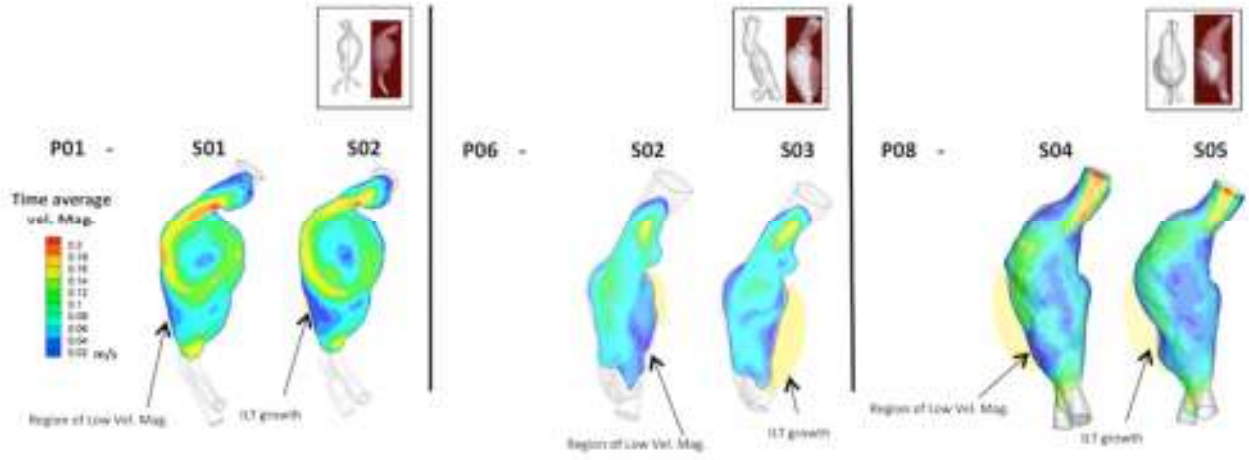

Figure 2.7 *Color contour of magnitude of time-averaged velocity plotted at particular longitudinal cross sections for P01, P06 and P08; respectively. Plots qualitatively show regions of low time-averaged velocity coincide with regions that experienced an ILT.*

An illustration of this is shown in Figure 2.7 when the magnitude of time-averaged velocity is plotted at specific longitudinal cross sections for 3 AAAs (P01 at scans 1 and 2, P06 at scans 2 and 3, and P08 at scans 4 and 5). From P06 and P08 it can be clearly seen that regions of low time-averaged velocity coincided with the regions of ILT accumulation. Another illustration of this trend is showed by P01 that experienced high

magnitude of time-averaged velocity near the wall in most of its lumen surface except at a small region; the same region at which, ILT accumulation was later seen. From the cross-sectional analysis (not shown here), it was also found that the direction of the flow at regions near the wall areas covered by ILT was dominantly aligned with the normal flow direction (from proximal to distal). However, reverse flow was seen at these areas at certain scans; nevertheless, these reverse flows realign with the normal flow direction at the following scans.

2.3.3.2 Wall shear stress

Differences in flow pattern found between AAAs with and without significant thrombus depositions were reflected in the TAWSS values. Figure 2.8 illustrated this effect by comparing TAWSS between 4 AAAs and a Healthy aorta. Results show that despite the fact that low TAWSS values were found in all AAAs in comparison to the healthy aorta; these values were lower in those aneurysms at the time that they developed a thick ILT. This trend was also captured when values of TAWSS at all AAAs' time points (scans) were average over the entire lumen surface, namely called "mean TAWSS", and plotted as a function of its maximum diameter.

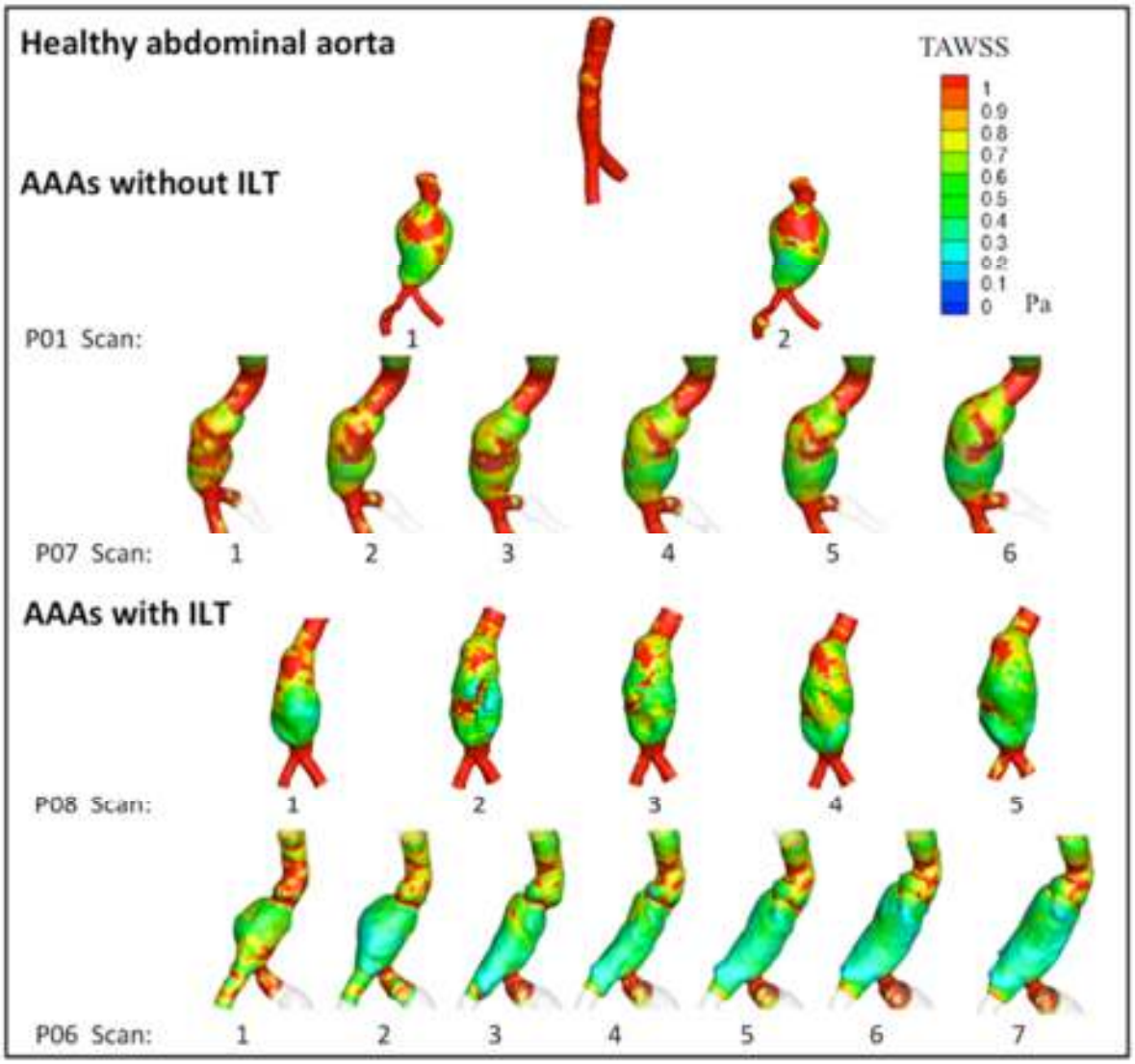

Figure 2.8 *Color-coded time averaged wall shear stress (TAWSS) for patients with and without ILT showing lower TAWSS values on AAAs with an ILT accumulation from those that did not developed thrombus.*

Figure 2.9a and Figure 2.9b shows these mean TAWSS values for groups of AAAs without and with ILT accumulation respectively. From these plots, it can be observed that AAAs with ILT deposition recorded lower mean TAWSS values than those without an ILT. Also, while a decreasing mean TAWSS trend as diameter increases was found in all AAAs

without ILT but patient P12 (Figure 2.9a), AAAs with ILT accumulation showed nearly constant values of TAWSS at larger diameters (Figure 2.9b).

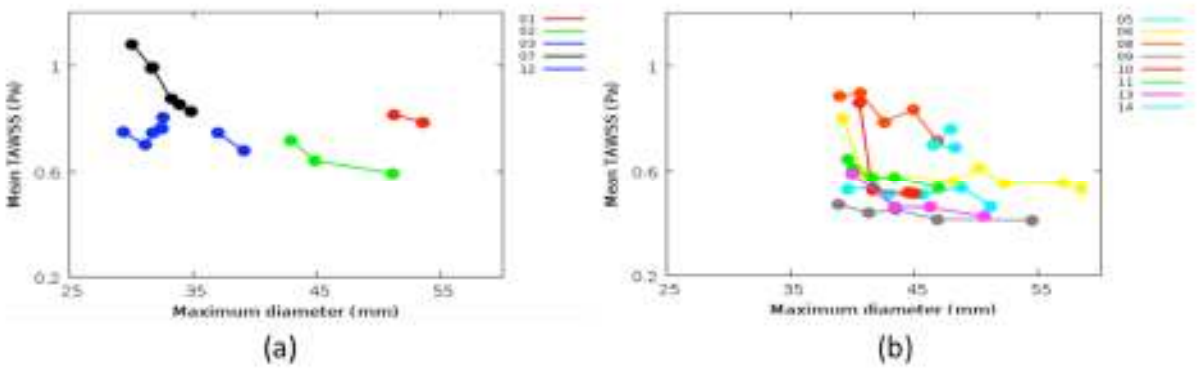

Figure 2.9 *mean TAWSS as function of maximum diameter of patients with (a) and without (b) ILT deposition*

2.3.4 ILT accumulation and wall shear stress relationship

The relationship between the ILT accumulation process and TAWSS was studied by plotting TAWSS values and ILT thickness for all lumen surfaces' nodal points of each AAA at each scan. Figure 2.10 illustrates the results for P8 and P9 and shows that ILT accumulated at areas of low TAWSS (yellow). It also showed that as ILT accumulates, the values of wall shear stress fluctuate within a low range. This trend was followed for all AAAs that developed significant ILT.

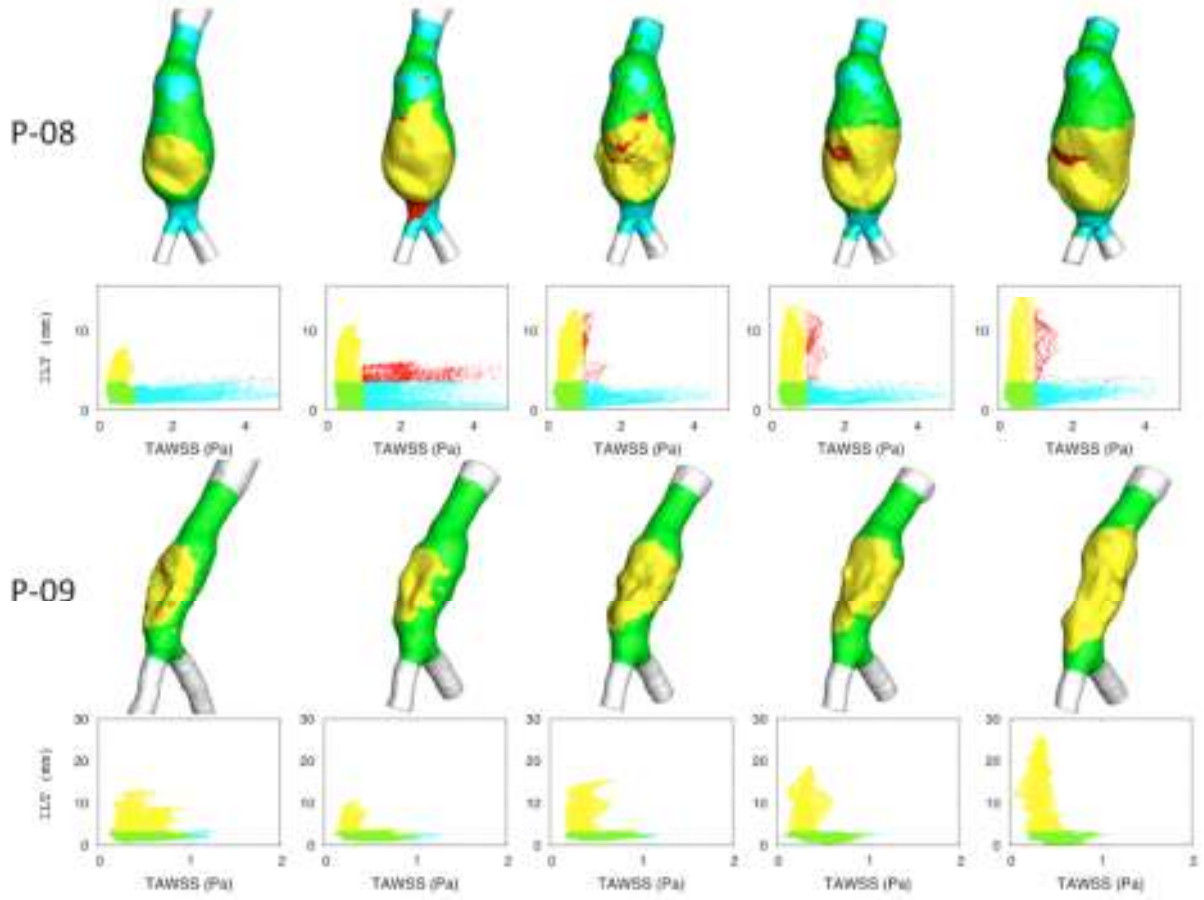

Figure 2.10 *TAWSS of all nodal points at each scan of P08 and P09. high TAWSS and low (cyan) or high (red) ILT thickness, and low TAWSS and low (green) or high (yellow) ILT thickness. (It shows that ILT accumulated at areas of low TAWSS (yellow).*

2.3.5 AAA expansion rates and ILT accumulation rates analysis

Using 29 samples from the group of AAA scans classified as "with an ILT", a linear regression was conducted for the ILT accumulation rate and AAA expansion rate, which revealed a positive linear correlation (R_{sq}=0.738; $\dot{AA}_{exp} = p1 * \dot{ILT}_{acum} + p2$; $p1 = 0.87 \pm 0.203$, $p2 = 10440 \pm 4335$; Figure 2.11). A statistical test of the null hypothesis that the slope of ILT accumulation rate is 1 from the result of linear regression gives us the value of t-statistics as 0.591 with the corresponding p-value as 0.559. This indicates that the ILT accumulation rate is statistically not different from the aneurysm expansion

rate (t=0.591, P=0.559). In other words, it was found that ILT accumulates at the same rate as the aneurysm expands.

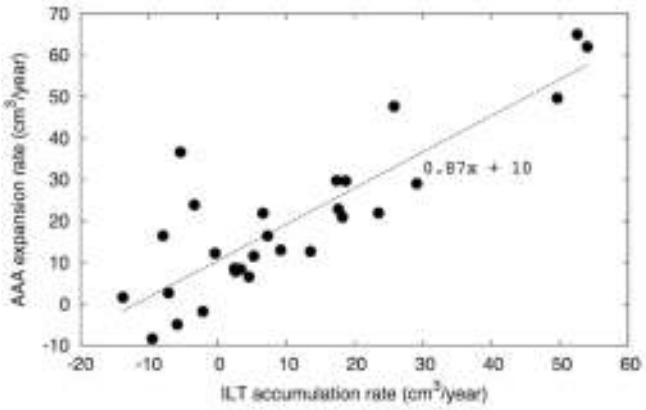

Figure 2.11 *Linear regression shows the linear positive correlation between ILT accumulation rate and AAA expansion rate (Rsq=0.738). (This plot shows that for these AAAs, ILT accumulates at the same rate that aneurysm)*

This finding and the positive correlation between ILT thickness and diameter reported above suggest that ILT might be occupying the expanded AAA areas, thus maintaining the lumen cross-section nearly constant. To confirm this, AAA and lumen cross-sectional areas at the region of maximum diameter were determined (Figure 2.12a). Analysis showed that, while the AAA cross-section area increased, the lumen cross-section area remained nearly constant. This relation is qualitatively (Figure 2.12b) and quantitatively (Figure 2.12c) shown for sequential scans at the region of maximum diameter for patients P-6, P-8, P-9 and P-11

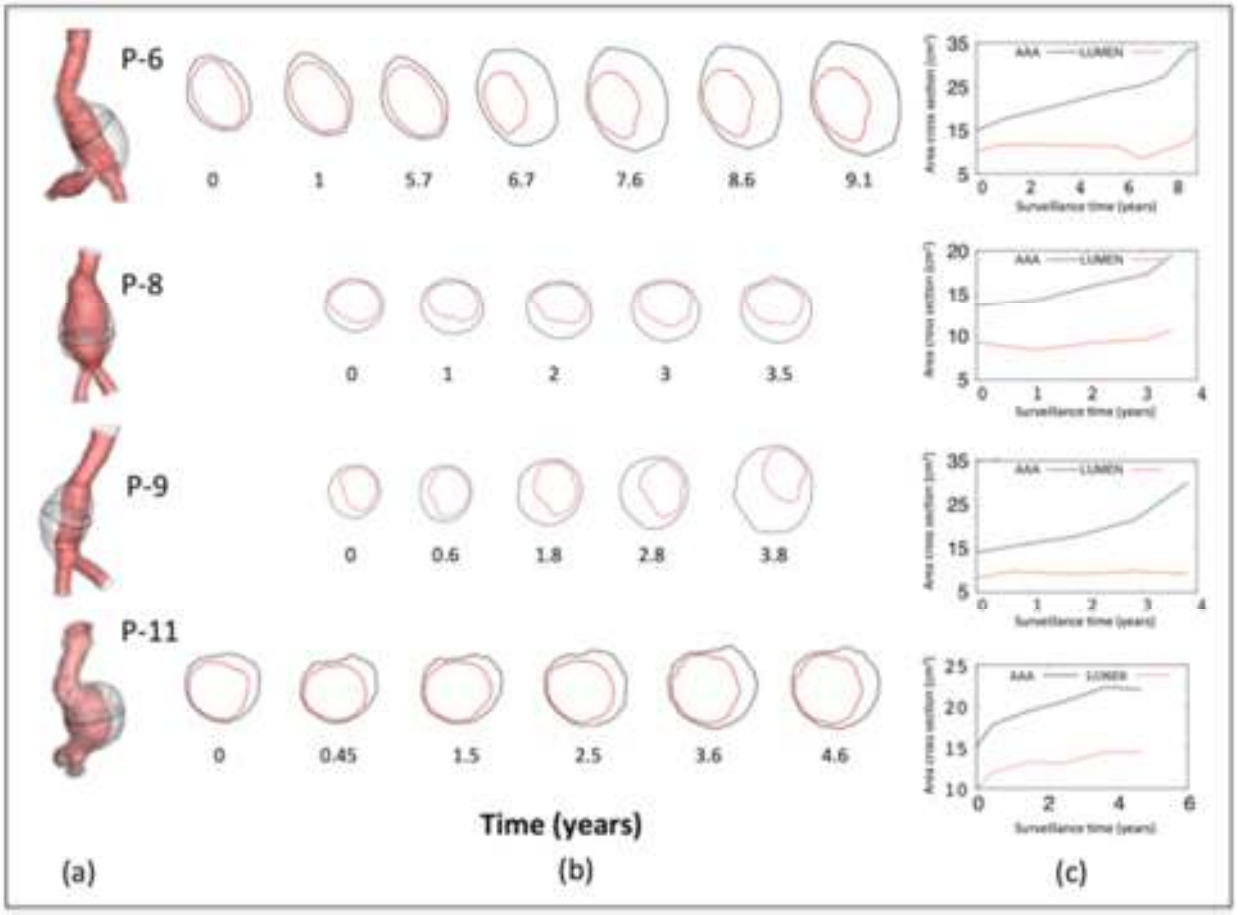

Figure 2.12 *Lumen and outer cross-sectional areas at regions of maximum diameter for AAAs P6, P7, P9, and P11. (a) region of maximum diameter, (b) increasing of the AAA cross-sectional outer area while the lumen area remained nearly constant, (c) Values of both cross-sectional areas at different times showing the same effect.*

2.3.6 Relationships between mean TAWSS, AAA expansion rate, and ILT accumulation rate

Results from mean TAWSS confirmed that AAAs classified as with an ILT showed lower mean TAWSS values than those that were classified as without ILT (Figure 2.13a-b).

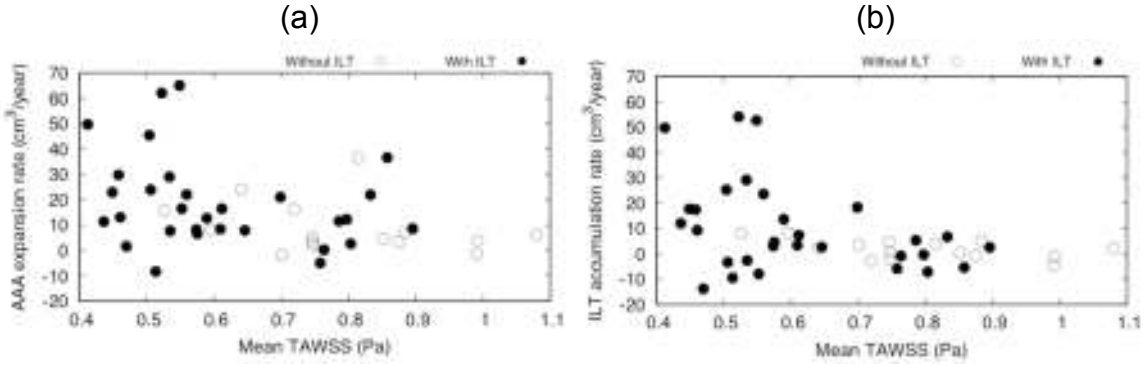

Figure 2.13 *Mean wall shear stress (TAWSS) values associated for AAAs with and without ILT associated with: (a) AAA expansion rate and (b) ILT accumulation rate. Here it can be seen that AAAs with no ILT have an overall higher mean TAWSS values than AAAs with an ILT accumulation. Conversely, higher values of ILT accumulation and AAA expansion rates were recorded in AAAs with an ILT accumulation that in turn also showed a lower mean TAWSS values.*

Comparing the results of mean TAWSS and the AAA expansion rate for these two groups of AAAs, it was observed that the highest expansion rates were recorded in patients that showed an ILT accumulation and lowest mean TAWSS values (Figure 2.13a).

A similar pattern was found when mean TAWSS values were compared to ILT accumulation rates (Figure 2.13b). Similar to the AAA expansion rates, the highest ILT accumulation rates were recorded at aneurysms with low mean TAWSS.

2.4 Discussion

This study used longitudinal CT images from 14 different patients and analyzed the relationship between the ILT accumulation process, wall shear stress changes, and AAA expansion. Results showed that the ILT accumulation process began at a localized region of maximum diameter and spread to neighboring regions while ILT continued to thicken at previously covered areas. While low wall shear stress showed to be a common feature on the regions where ILT deposition occurred, the rate at which ILT accumulated occurred

at the same rate as the aneurysm expansion. Comparison between AAAs with and without thrombus showed that aneurysm with ILT recorded lower values of wall shear stress and higher values of AAA expansion than those AAAs free of thrombus.

The dynamics of the ILT accumulation process is here described for the first time using a macroscopic perspective. Briefly, ILTs were most often found accumulating eccentrically in the AAA [42], and their localization and initial accumulation were both observed in regions of maximum diameter. The continuous ILT thickening and outward spreading pattern described here agrees with the hypothesis that the luminal layer is active and interacts with the main blood flow, which might enhance further thrombus accumulation [31].

The ILT accumulation process described above for AAAs that showed an ILT buildup in conjunction with the positive correlation seen between ILT thickness and diameter suggests that ILT accumulates at the AAA regions that have expanded, agreeing with what Wilson and colleagues [78] hypothesized. Therefore, it is expected to find larger ILT volumes at larger diameters, as it was found by Hans and colleagues [42]. This trend, however, cannot be generalized for all aneurysms since our results showed a few AAAs that despite their large size, were found free of thrombus. Interestingly, in these AAAs, mean TAWSS values were higher than in those AAAs that developed a thick ILT. This result suggests that high values of wall shear stress would prevent the ILT from accumulating. It has been previously proposed that increasing the values of wall shear stress would attenuate AAA growth [51]. Our results would additionally suggest that by increasing wall shear stress values e.g., by exercising, ILT deposition could also be prevented.

On the other hand, once this ILT process begins, it accumulates at the same rate that AAA expands; maintaining the lumen area nearly constant. This nearly constant area would also impact hemodynamic conditions. In fact, our results showed that values of TAWSS on average would remain nearly constant on aneurysms of larger diameters. In other words, all these findings indicate that while low values of wall shear stress are promoting ILT accumulation; the thrombus accumulation may be at the same time modifying values of wall shear stress.

The effect of ILT on AAA prognosis has also been studied by other using different approaches[10,25,34,49,52,54,72,74,77] and the possible association between thrombus accumulation and AAA growth has been proposed [70]. Our results agree with the suggestion of an association between ILT and AAA growth since higher values of aneurysm expansion rate were recorded on AAAs with an ILT accumulations in comparison to those that remained free of thrombus. It is worth noting that these AAAs that showed higher expansion rate values were in turn AAAs that showed lower values of wall shear stress.

The positive association between aneurysm size and AAA expansion has been widely proposed and the relationship between wall stress and strength is expected to be linear and gradually changing as the aneurysm progresses [14,73]. The hemodynamic forces, however, responsible of imposing the wall shear stress also change [29,30,63]. Albeit multiple hemodynamic factors (oscillatory shear index, endothelial cell activation potential or thrombus activation potential[5,22]) along with the wall shear stress have been proposed as key factors in the accumulation process and further AAA expansion.

Once ILT is initially adhered to the lumen wall, it would enhance the adhesion of new fresh thrombus at regions where wall shear stress is favorable for its adhesion (low WSS regions). This adhesion would in turn activate proteolytic degradation with stress-mediated growth [7] that modifies the AAA wall stress and strength [10,25,34,49,52,54,72,74,77]. Therefore, as AAA expands, ILT would accumulate and spread throughout the AAA sac modifying the wall stress-strength relationship strongly. At the same time, the ILT accumulation would promote a reduction of the lumen passage, which in turn would have an impact in the hemodynamic conditions. These hemodynamic conditions would be lowering gradually as AAA expands and thus promoting further accumulation. In summary, once ILT begins to accumulates, it would slowly impact the wall-strength relationship and potentially enhancing AAA expansion while modifying wall shear stress levels. This WSS level would be also modified by AAA expansion

Like most human studies, this investigation had limitations that need to be considered while interpreting the results. This study used sequential CT scans from 14 patients, and it would be ideal to increase the sample size to reach stronger conclusions. Additionally, it was difficult to accurately differentiate the aneurysm wall from the thrombus layer [68]. This required the summation of ILT and AAA wall thicknesses and that a uniform 3mm AAA wall thickness was assumed for analysis. This assumption could have over- or underestimated the value of the ILT thickness. The results for hemodynamic simulations of this study were obtained based on volumetric flow rate of a young healthy aorta. Although the volumetric flow rate and pressure wave as inlet and outlet are commonly used for setting up the boundary conditions [6,7], the evolution of AAA may have effects on the total rate or profiles of inlet and outlet flow and quantitative measurements of flow

rates for individual patients will be needed for better estimation of the blood flow. Also, while a laminar flow assumption was made in these hemodynamic simulations relying on a global Reynolds number estimated at the inlet, there is a possibility that flow might become turbulent at some regions during cardiac cycle. Despite the limitations that these assumptions could have instilled, results in this study are consistent with previous findings.

In closing, this study used longitudinal studies of 14 patients and analyzed the relationship between ILT accumulation, wall shear stress and AAA expansion. The findings presented explained the ILT accumulation process and showed that ILT accumulated at the same rate as the AAA expansion rate. Additionally, our results support the idea that suggests that low wall shear stress level would promote ILT deposition and submits the hypothesis that by increasing wall shear stress levels thrombus accumulation inside AAA can be avoided.

CHAPTER 3

Association of regional ILT changes with local hemodynamic variables: TAWSS, OSI, and vortical structures

3.1 Introduction

In our previous analysis, we showed that lower values of mean TAWSS were recorded in AAAs with ILT deposition in comparison to those without ILT. This suggests a potential relationship between TAWSS and ILT deposition. Motivated by this finding, a local association between the local hemodynamic environment and local changes in thrombus was explored.

Previous studies have analyzed this association at specific AAA regions[5,22,23], proposing different hemodynamic variables to be important in the ILT accumulation process. For instance, some studies have suggested that variables as TAWSS [26,82], oscillatory shear index (OSI) [5], and endothelium activation potential (ECAP) [22] could potentially being used to predict the ILT accumulation process.

Recent other studies suggested that vortical structures might play an important role in thrombus accumulation [27]. However, it is not well understood mechanisms by which the vertical structure enhances to transport the activated platelets to distal AAA regions where thrombus accumulation and how those vortical structure is related to hemodynamics parameters.

Those previous results from these analysis, however, are still inconclusive because of the small data. There is, hence, a need to test multiple hypotheses on various hemodynamic variables using a large data set and thus clarify the potential association between each local hemodynamic variable and local changes in ILT. Specially using high-

resolution patient-specific information of the changes in thrombus accumulation associated to local hemodynamic conditions.

In this chapter, the local association among all the above proposed parameters (i.e. vortical structures, WSS, OSI, and ECAP) and local changes of thrombus thickness was analyzed to test their potential associations to the thrombus accumulation process. Results from the analysis in this chapter revealed that vortical structures that typically form at the proximal AAA regions were found to consistently dissipate near zones where positive changes in ILT thickness were recorded. On these lumen wall regions, correlation analysis showed that among all tested hemodynamic variables, TAWSS showed to be the most correlated.

3.2 Methods

3.2.1 ILT thickness and its changes

The ILT thickness distribution ($ILT^i(\boldsymbol{x_1})$) projected on either AAA outer or lumen surface at each scan "i" of each AAA was estimated in our previous analysis. Here, we used these values to quantify the changes of ILT thickness (ΔILT). These changes ($\Delta ILT(\boldsymbol{x_1}) = ILT^{i+1}(\boldsymbol{x_1}) - ILT^i(\boldsymbol{x_1})$) were estimated by mapping $ILT^i(\boldsymbol{x_1})$ at time-point "i" to $ILT^{i+1}(\boldsymbol{x_1})$ at the next time point "$i+1$" (Figure 3.1). To map from the point $\boldsymbol{x}^i$ to $\boldsymbol{x}^{i+1}$, we utilize the AAA centerlines previously generated and a 2D parametrization $\boldsymbol{x}^i = \boldsymbol{x}^i(S, \theta)$. Here coordinates S and θ represents the length along the centerline and circumferential angle; respectively. Thus, a subset of MxN points $\boldsymbol{x_1} \in \Gamma_l$ were chosen, (where M=number of center-points along the centerline and N=360) to estimated and express ΔILT in the 3D spatial coordinate $\Delta \boldsymbol{ILT}(\boldsymbol{x}, \boldsymbol{y}, \boldsymbol{z}) = \Delta \boldsymbol{ILT}(S(s, \theta), \theta(s, \theta))$.

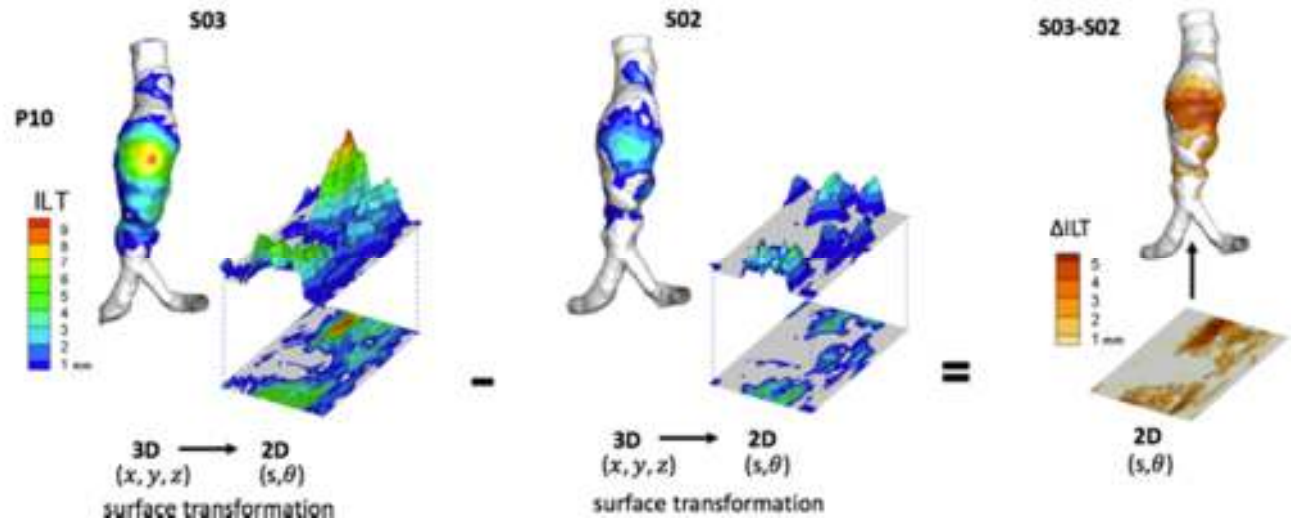

Figure 3.1 *Estimation of ΔILT by mapping a subset of MxN (M= centerpoints along C and M=360) points $x_1 \in \Gamma_l$ using a 2D parametrization $x^i = x^i(C, \theta)$ which was expressed in the 3D spatial coordinate $\Delta ILT(x, y, z) = \Delta ILT(S(s, \theta), \theta(s, \theta))$*

3.2.2 Vortex eduction

These are coherent structures that commonly appear in large arteries (Re > 100) [8] and might be responsible for the particle transport (like RBC, WBC and platelets) and for the mixing chemical species in AAAs. These particle transports might influence the thrombus accumulation process. Up to date, the exact mathematical expression that defines these vortices are still debated. The most common method used to characterize vortical structures is known as "λ2 method" [48]. This method defines vortical structures as regions of non-zero vorticity surrounding a pressure minimum. This is achieved by using the reduced form of the Navier Stoke equation (Eq. 6). This reduced form is obtained by taking the gradient of the Navier-Stoke equation and by dropping the inertial and viscous terms:

$$\boldsymbol{D}^2 + \boldsymbol{\omega}^2 = -\frac{1}{\rho}\nabla(\nabla p), \tag{3.1}$$

where:

$$\nabla \boldsymbol{v} = \boldsymbol{D} + \boldsymbol{\omega}\ , \tag{3.2}$$

$$\boldsymbol{D} = \frac{1}{2}(\nabla \boldsymbol{v} + \nabla \boldsymbol{v}^T) \qquad \text{and} \qquad \boldsymbol{\omega} = \frac{1}{2}(\nabla \boldsymbol{v} - \nabla \boldsymbol{v}^T), \tag{3.3 a-b}$$

where $\boldsymbol{D}$ and $\boldsymbol{\omega}$ represent the symmetric and antisymmetric parts of the velocity gradient tensor. This method defines vortices as regions with negative eigenvalues of the tensor $\boldsymbol{D}^2 + \boldsymbol{\omega}^2$. Since this tensor is symmetric, eigenvalues will be always real. Then if $\lambda_1, \lambda_2, \lambda_3$ are the eigenvalues of this tensor and ranking these eigenvalues as $\lambda_1 > \lambda_2 > \lambda_3$, the vortices is visualized when $\lambda_2 < 0$.

3.2.3 Local hemodynamic parameters calculations

Estimation of local hemodynamic variables such as TAWSS and oscillatory shear index (OSI) were obtained through computational fluid dynamics (CFD) to lumen all volumes from all AAA' scans (n=40; Figure 1.1). These variables represent the time averaged magnitude and direction of the shear stress vector; respectively. The mathematical definition of OSI is defined as follows:

$$OSI = \frac{1}{2}\left(1 - \frac{\left\| \int_{T_1}^{T_2} \boldsymbol{wss}\, dt \right\|}{\int_{T_1}^{T_2} \|\boldsymbol{wss}\|\, dt}\right) \tag{3.4}$$

this variable ranges between 0 and 0.5, where Its maximum value represents a purely oscillatory flow with equal magnitude of WSS in both direction, while its lower value represents unidirectional flow condition.

An additional parameter that measures susceptibility of the endothelium cell to promote thrombus accumulation called "endothelial cell activation potential" (ECAP) [22,23] is being proposed to better predict the accumulation of thrombus. This metric is defined as the ratio of the two previously defined indexes (e.g. TAWSS and OSI) as follows:

$$ECAP = \frac{OSI}{TAWSS}\,. \tag{10}$$

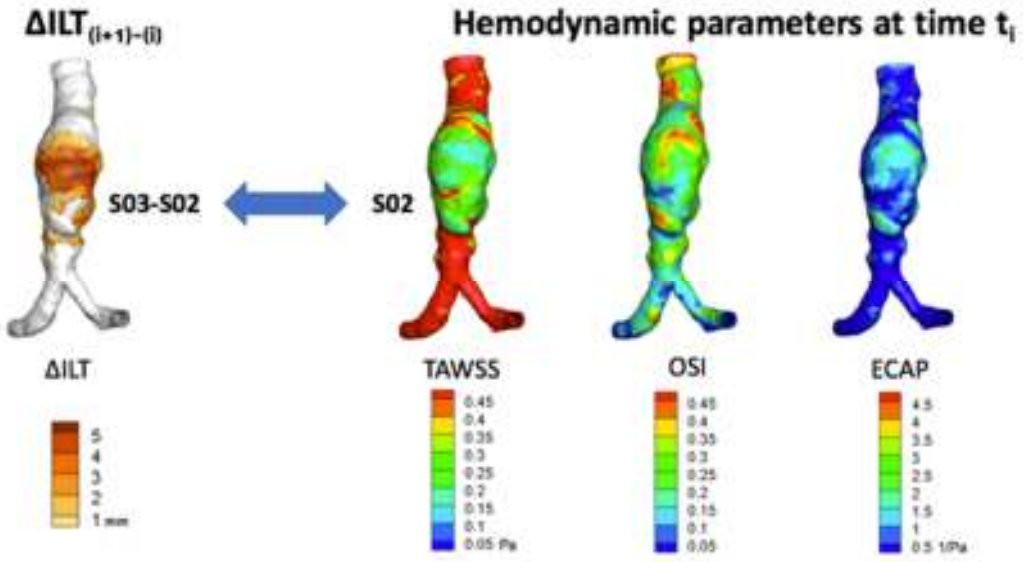

Figure 3.2 *Locations of ∆ILT associated to local hemodynamic conditions of TAWSS, OSI and ECAP for P10 at time-point 2 (scan 2)*

The hemodynamic parameters (TAWSS, OSI, and ECAP) were plotted for P10 in S02 and $\Delta\boldsymbol{ILT}$ is estimated from S02 to S03, shown in Figure 3.2.

3.2.4 Statistical analysis of the relationship among parameters

The relationship between local hemodynamic parameters at time point "i" and changes in thrombus thickness from $ILT^{i}(\boldsymbol{x_1})$ to $ILT^{i+1}(\boldsymbol{x_1})$ (Figure 3.2) was tested on each AAA at each time-point. AAA at each time-point. A Pearson correlation coefficient per scan was computed using a subset of nodal points that was used to record changes in ILT thickness ($\Delta ILT \neq 0$). This resulted in a table of 40 correlation coefficients describing the relationship between hemodynamic and thrombus parameters at each time-point. The calculation of coefficients is performed using the Matlab software (Mathwork, Natick,

USA). Each correlation coefficients was classified as strong (r >0.5), moderate (0.3<r<=0.5), and weak (0.1<r<=0.3) according to guidelines provided by Cohen et al [19].

3.3 Results

3.3.1 Vortical structures

Our results showed that vortices that formed at the proximal regions during the systolic phase (figure 5), were later detached from the wall, transported downstream where they broke-up and dissipated during the diastolic phase. An illustration of these vortical structure pattern is shown in Figure 3.3a for AAA P10 at scan 01. Here it can be seen a large vortical structure that formed at the proximal region, translated while splits in smaller vortices, and dissipated at regions where positive changes in ILT thickness was observed. Another similar example is shown for AAA P05 at scan 05 (figure 3.3b.), however, this AAA showed multiple large vortices forming at the proximal region that split in smaller vortices. Nevertheless, all these vortices also dissipated at regions of positive ILT thickness changes.

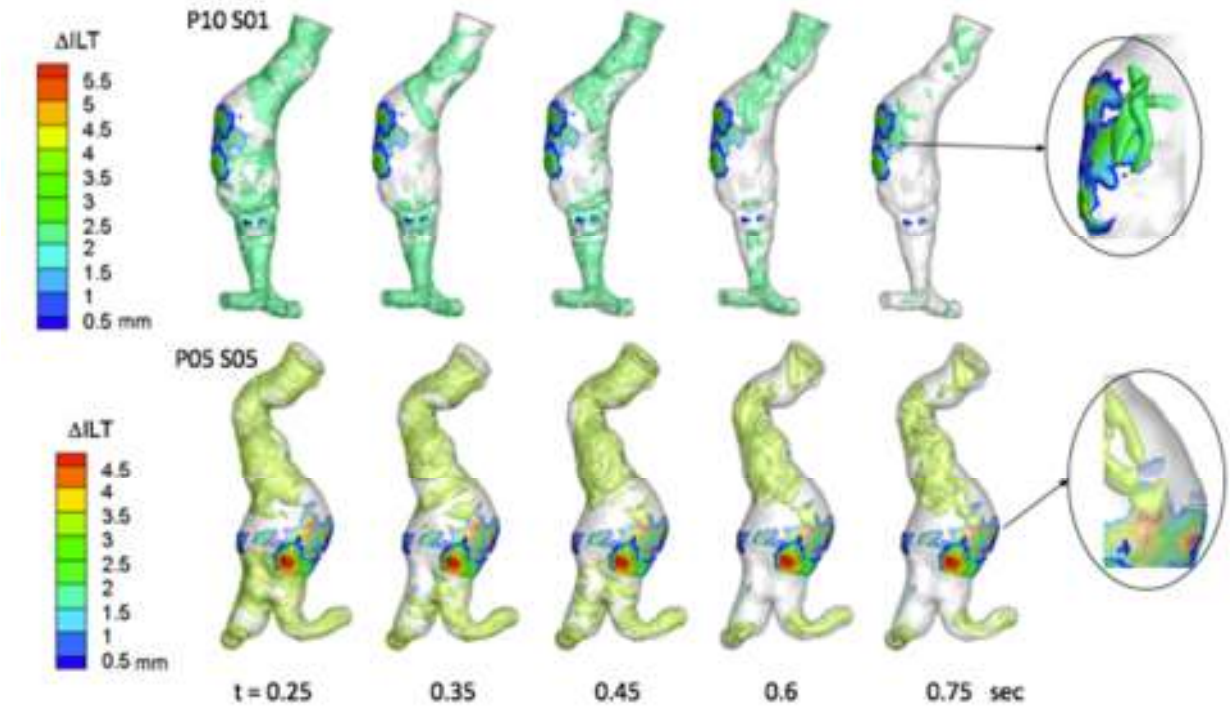

Figure 3.3 *Eduction of vortical structures in AAAs that showed a thrombus deposition (P10-S01 and P05-S05). In these AAAs vortical structures form at the proximal regions and dissipate at zones of thrombus accumulation at approximately end diastolic.*

Similarly to AAAs that showed an ILT accumulation, vortical structures were also seen in AAAs that did not show thrombus deposition. In these AAAs, however, vortical structures showed to be stronger than in AAAs that showed thrombus accumulation, swiping the majority of the AAA luminal wall. Figure 3.4 shows vortical structures pattern for P01 at scan 01. This AAAs showed that due to the stenotic region found at the proximal part, a strong vortex forms during the peak systolic (t=0.25). This vortex moves and sweeps most of the lumen surface during the rest of the cardiac cycle.

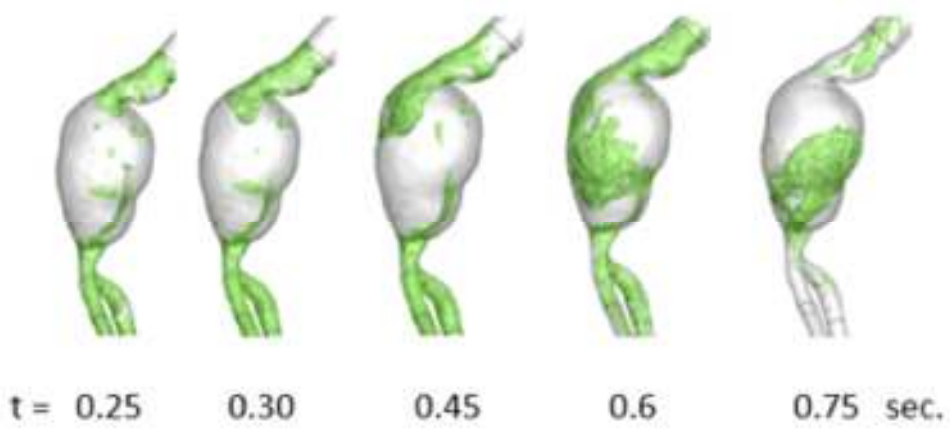

Figure 3.4 *Eduction of vortical structures in AAA without an ILT accumulation (P10-S01). In this AAA, a strong vortical structure is formed due to an stenotic area at the proximal region. This vortex swipes the entire lumen surface promoting a high wss environment*

These differences vortical structure patterns could affect TAWSS values. This is seen in figure 3.5 in which spatial distribution of TAWSS is shown for AAAs with (P10 S02) and without (P01 S01) a thrombus accumulation. Here it can be seen that while P01 the vortices that swipes the entire lumen surface influence values of TAWSS in comparison to the AAA that experience a dissipation of the vortex formed at the proximal region.

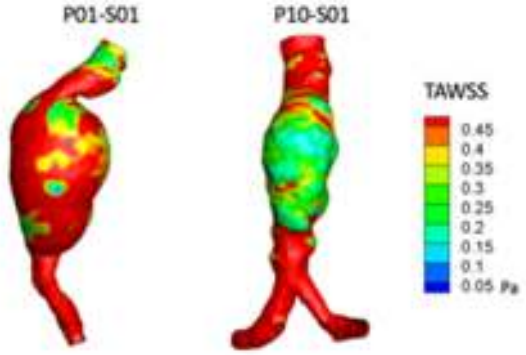

Figure 3.5 *Spatial distribution for P01-S01 and P10-S01 showing the effect of the vortical structures on TAWSS values.*

3.3.2 Statistical analysis

Results from the correlation coefficient analysis to test the local relationships between hemodynamic parameters (TAWSS, OSI, ECAP) and ΔILT on each AAA at all time-points was performed and it is presented in Table 3.1

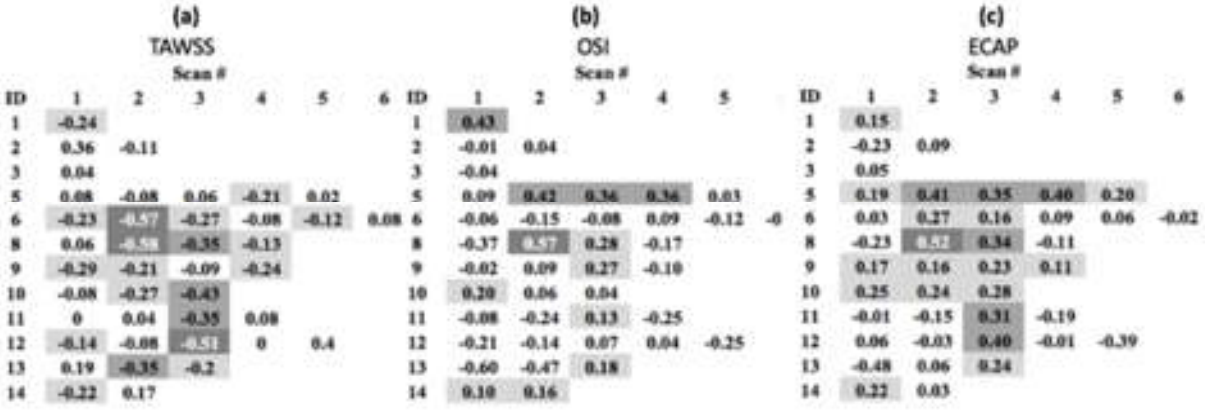

(a) TAWSS							(b) OSI							(c) ECAP						
	Scan #							Scan #							Scan #						
ID	1	2	3	4	5	6	ID	1	2	3	4	5		ID	1	2	3	4	5	6
1	-0.24						1	0.43						1	0.15					
2	0.36	-0.11					2	-0.01	0.04					2	-0.23	0.09				
3	0.04						3	-0.04						3	0.05					
5	0.08	-0.08	0.06	-0.21	0.02		5	0.09	0.42	0.36	0.36	0.03		5	0.19	0.41	0.35	0.40	0.20	
6	-0.23	-0.57	-0.27	-0.08	-0.12	0.08	6	-0.06	-0.15	-0.08	0.09	-0.12	-0	6	0.03	0.27	0.16	0.09	0.06	-0.02
8	0.06	-0.58	-0.35	-0.13			8	-0.37	-0.57	0.28	-0.17			8	-0.23	-0.52	0.34	-0.11		
9	-0.29	-0.21	-0.09	-0.24			9	-0.02	0.09	0.27	-0.10			9	0.17	0.16	0.23	0.11		
10	-0.08	-0.27	-0.43				10	0.20	0.06	0.04				10	0.25	0.24	0.28			
11	0	0.04	-0.35	0.08			11	-0.08	-0.24	0.13	-0.25			11	-0.01	-0.15	0.31	-0.19		
12	-0.14	-0.08	-0.51	0	0.4		12	-0.21	-0.14	0.07	0.04	-0.25		12	0.06	-0.03	0.40	-0.01	-0.39	
13	0.19	-0.35	-0.2				13	-0.60	-0.47	0.18				13	-0.48	0.06	0.24			
14	-0.22	0.17					14	0.10	0.16					14	0.22	0.03				

Table 3.1 *Correlations between ∆ILT and (a) TAWSS, (b) OSI, and (c) ECAP for each scan of each AAA*

Results from the analysis showed that among all the proposed parameters, TAWSS not just showed an overall inverse correlation in most of AAAs' scans, but also recorded stronger correlations in comparison to the other variables. Specifically, from all the scan tested (n=40), approximately half of them (52.5%) depicted an overall inverse correlation (Figure 3.6a). This overall correlation included strong, moderate and weak correlations (7.5, 10 and 35%; respectively; Figure 3.6b).

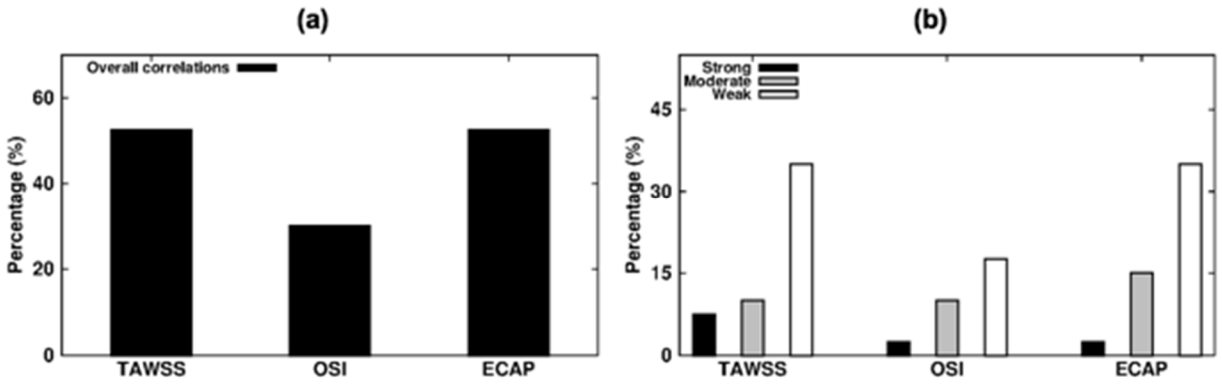

Figure 3.6 *Percentage of number of scans showing an (a) overall and a (b) strong, moderate and weak correlations between ∆ILT and TAWSS (Pa), OSI and ECAP (1/Pa), respectively*

Another variable that showed similar results was ECAP. Correlation coefficients also showed an overall direct correlation in 52.5% of the tested scans, however, less scans showed to be strongly correlated (2.5% of scans; 3 vs 1 strongly correlated scans) in comparison to the correlations found when ΔILT-TAWSS relationship was tested. Lastly, results from the correlation analysis performed to test the ΔILT-OSI relationship showed that 30% of the tested scans showed an overall direct correlation.

3.3.3 Regional relations among hemodynamic parameters and thrombus thickness changes

Spatial distribution of the proposed hemodynamic quantities estimated at times i were qualitative analyzed in regions where positive changes in thrombus thickness ($\Delta ILT > 0$) between times i and $i + 1$ were observed. This analysis revealed common trends in some hemodynamic parameters. This is the case of the TAWSS that showed to be consistently low in regions of positive ΔILT (TAWSS < 0.4 Pa; Figure 3.7). As an example, we have P12 at scan 3 showed that regions of positive thrombus accumulation (ΔILT>0) correlated

with regions of low TAWSS. Interestingly, some of the region largest accumulation occurred at region of lowest TAWSS (Figure 3.7).

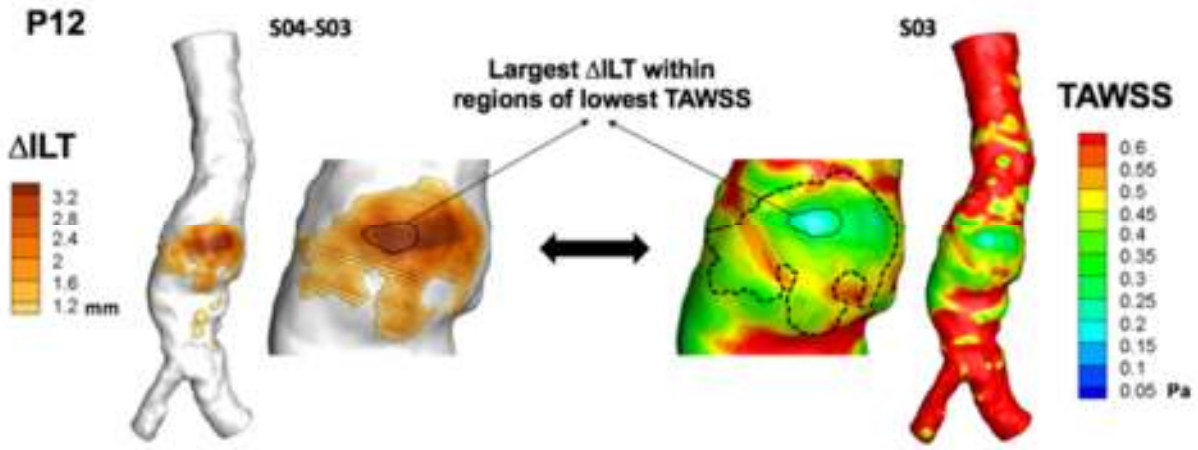

Figure 3.7 *Spatial distribution of ΔILT and TAWSS for P12 at scan 3 showing deposition occurring at regions of low TAWSS. Here, regions of largest ΔILT occurs within region of lowest TAWSS*

Similar to the relationship to TAWSS, local changes in thrombus were also qualitative associated to estimated values of ECAP. Results of this analysis showed that in some scans of some AAAs, regions of positive ΔILT were associated to high values of ECAP. As an illustration, we have P10 at scan 2 (Figure 3.8) that shows regions of positive accumulation at zones where high values of ECAP were recorded. Similar to TAWSS, higher values of ECAP also coincided with regions of larger accumulation on these AAAs (Figure 3.8).

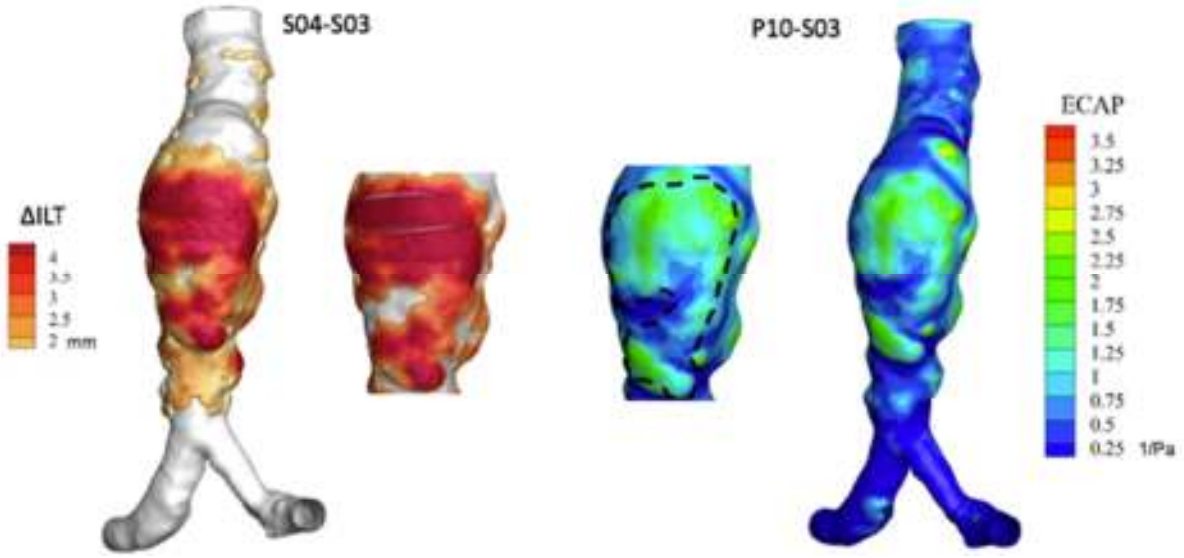

Figure 3.8 *Spatial distribution of ∆ILT and ECAP for P12 at scan 3 showing deposition occurring at regions of high ECAP. Here, regions of largest ∆ILT occurs within region of higher ECAP zones.*

Spatial distribution of OSI was also qualitative associated to ∆ILT. As an illustration of the association found we have P08 at scan 2 (Figure 3.9). This AAA at that specific scan (S02) shows that positive values of ∆ILT are seen at regions where high values of OSI were also observed. This AAA also showed to be qualitative associated to regions of low values of TAWSS (Figure 3.9c) and high values of ECAP (figure 3.9d); respectively. Observation on this AAA scan agree with the strong correlation coefficients found between ∆ILT and all tested variables.

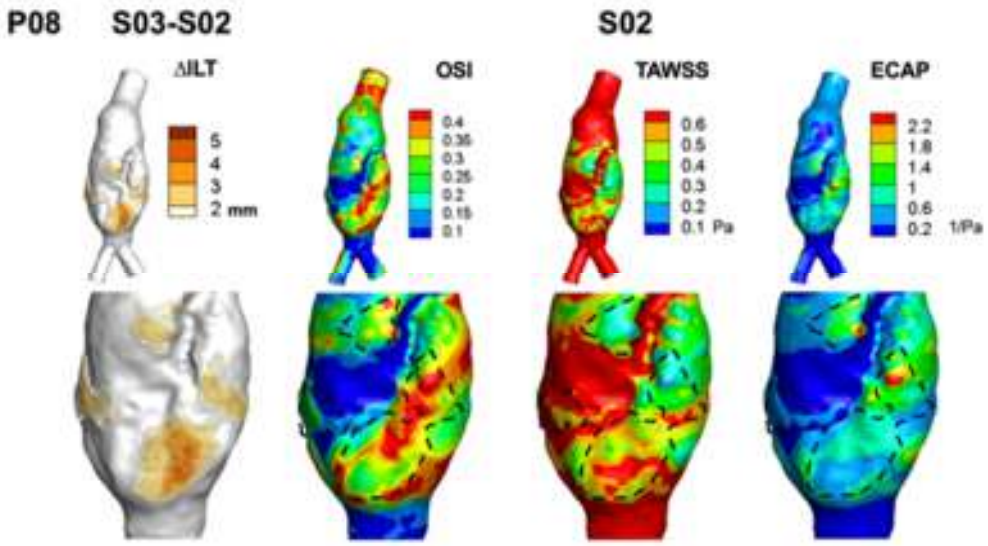

Figure 3.9 *Spatial distribution of ∆ILT, OSI, TAWSS and ECAP for P08 at scan 2 showing deposition occurring at regions of high b) OSI, c) ECAP and b) low TAWSS*

Some scans, however, large changes in ILT thickness at both high and low OSI. This is the case of P05 at scan 1 (Figure 3.10) that depicted two regions of large accumulation occurring either at high and relatively low OSI zones.

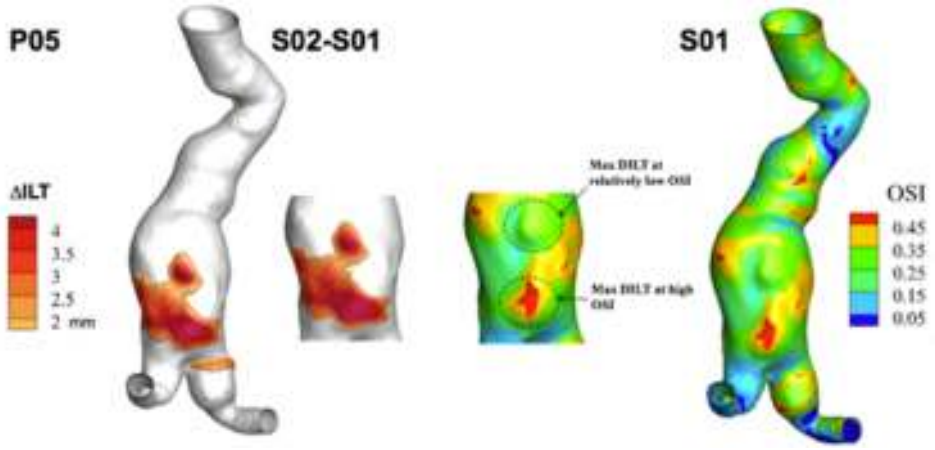

Figure 3.10 *Spatial distribution of ∆ILT and OSI for P05 at scan 1 showing deposition occurring at regions of high and relatively low OSI.*

3.4 Discussion

In this chapter, local changes in thrombus thickness were estimated and associated to vortical structures and local hemodynamic variables, qualitatively and quantitatively. Local ILT changes were estimated by mapping points between time-point "i" to time-point "$i+1$", while vortical structures and local hemodynamic variables such as TAWSS, OSI and ECAP were derived from CFD simulations at time point "i". These variables were ultimately used to perform a correlation study using Pearson correlation coefficients. Results revealed that vortical structures that typically form at the proximal AAA regions were found to consistently dissipate near zones where positive changes in ILT thickness were recorded. On these lumen wall regions, correlation analysis showed that among all tested hemodynamic variables, TAWSS showed to be the most correlated.

Vortical structures are characteristic flow patterns that describes a non-organized flow. These coherent structures are being suggested to play an important role in the thrombus accumulation process [17]. In a normal aorta, small spanwise vortices that roll up due to the aortic undulation are commonly seen during the early stages of the systolic phase [8]. In AAAs, our results also showed spanwise vortices forming at the proximal region during the systolic phase. These vortices, however, became stronger as they detached from the aortic wall right before entering the aneurysm bulge and dissipated during the diastolic phase at specific near wall regions. Interestingly, our results found that the dissipation regions coincided with those zones where positive changes in ILT thickness was observed. This finding agrees with the hypothesis that suggests that vortical structures would convect and concentrate platelets and other blood factors (e.g. Thrombin) on regions of ILT accumulation [9].

While vortical structures are being suggested to have an influence on the local hemodynamic environment [8], potentially affecting the accumulation of thrombus [17], it is not always the case. In the flow pattern of P01-S01 (Figure 3.4, 3.5), the vortex moves and sweeps most of the lumen surface during the rest of the cardiac cycle, contrast to the impinging flow in Fig. 3.3 in which the sweeping flow on the lumen surface could potentially prevent the accumulation of thrombus. This was found when vortices in AAAs with and without ILT were compared. Specifically, this comparison found that while both AAAs were affected by strong vortical structures, vortices in the AAA without ILT swiped most of the lumen surface, promoting higher levels of WSS. Those pattern of vertical structure with high WSS levels could, potentially avoid the accumulation of thrombus.

This finding motivated us to perform a correlation analysis to study the relationship between local values of time averaged WSS (TAWSS) and other hemodynamic parameters (OSI and ECAP) with local changes of thrombus thickness. These relationships were tested on each AAA at all time-point available. Results from the analysis showed that among these parameters, TAWSS showed an overall inverse correlation in about half of the scan tested (52,5% of all scans tested), shown in Figure 3.6a. At those low wall shear stress levels, antithrombotic agents have been proven to be effective and shear dependent (< 600sec-1) [62]. This would regulate the platelet aggregation mediate by fibrinogen biding GPIIb/IIa [40] and therefore the formation of thrombus.

Another parameter that has being lately proposed as potential predictor of ILT accumulation is ECAP [22,23]. This variable defined as the ratio between TAWSS and OSI was proposed from the premise that activated platelets would adhere onto low WSS

regions near recirculation zones (high OSI) [7]. This variable was also correlated with ΔILT and results showed that, similarly to the results found with TAWSS, about half of the scans also showed a correlation.

As any other analysis, this study also encounter some limitations. For instance, at the time of mapping nodal points between two consecutives scans. The mapping was achieved by assuming that centerline angles and lengths were constant between two consecutives scans. Although sensitivity analysis previously performed showed not significant differences in centerline length and angle, these small changes could potentially affect the ΔILT calculation. Another limitation arise at the time longitudinal studies were acquired. Since these studies were acquire retrospectively the time between consecutives scans could not be controlled. This could also potentially weaken our statistical analysis. Despite these limitation, correlation trends between local hemodynamic parameters and changes in thrombus thickness were achieved and those agree with suggested hypothesis.

In summary, this analysis used CFD and ILT thickness information from our previous analysis and study the relationship between hemodynamic parameters with local quantified changes in ILT thickness. These results suggest that vortical structures might be concentrating platelets and chemical species responsible for the formation of thrombus (e.g. Thrombin) at regions where ILT accumulation takes place. Results also submits the idea that although TAWSS is not the only parameters involved in the formation of thrombus, in some cases, this variable could regulate its accumulations.

CHAPTER 4

Quantification of the shear history of platelets, and their association with local changes of ILT thickness

4.1 Introduction

The specific mechanisms leading to the initiation of thrombus inside AAAs is still unknown. A widely accepted hypothesis suggests that platelets, due to the recirculation regions commonly found inside AAAs, would be exposed to high shear environments and as a result would activate. Chap 3, however, found that thrombus accumulation occurred in a low TAWSS and other studies proposed that activated platelets would recirculate at low velocity regions where accumulation occurs [22,23]. This hypothesis, however, has been lately challenged and instead an activation of platelets due to a thrombo-active surface is being proposed [5,9,43]. With conflicting two different hypotheses, there is a need to elucidate whether mechanically induced platelet activation is a key mechanism leading to the formation of thrombus.

The activation of platelets due to high shear rates comes from a theory of damage [2]. The theory, initially proposed while studying of hemolysis due to high shear [15,69], was found to have a similar phenomenological effect on platelets [65]. Specifically, once a platelet reaches these activation/damage shear stress levels, it would release adenosine diphosphate (ADP), serotonin, von willebrand factor (vWF) among other chemical species, many of which, would promote platelet activation and aggregation [56].

The mechanical activation of platelets has been experimentally studied and all agree that an activation of platelet would not be just a function of the stress but also of the time a platelet is being exposed to such stresses[61,80]. This cumulative effect is being

study by Hellum et al [45] and they have presented a plot that depict the activation locus at different stress and times using a power law relationship.

Many computational models have also tried to model this effect. For example, an early model, approached the activation by using a linear stress-exposure time model [11]. These models are being lately replaced by power law model that according to literature better reflects results obtained through experimentation [41].

In AAAs, several approaches have been used to test this hypothesis [6,22,23,43]. For instance, a hemodynamic parameter such as platelet activation potential (PLAP) and thrombus formation potential (TFP) based on this theory are being proposed to be better predictors of ILT accumulation [22]. However, none of these parameters have been estimated using a more complex platelet activation model (power law) nor validated using a large patient-specific data set. In addition, there is still uncertain whether shear rates levels and the time that platelets are exposed to such stresses would promote platelet activation.

Hence, in this chapter, levels of activation will be estimated using a Lagrangian particle method with a power law platelet activation model. Also, spatial distribution of PLAP and TFP on regions where changes in ILT was observed will be correlated using a Pearson correlation coefficients. Results from the analysis in this chapter revealed that just 22.5% and 30.0% of the scans showed an overall correlation between changes in ILT, PLAP and TFP, respectively. Also, results from measuring the activation levels in all AAAs showed that none of the aneurysms tested showed activation levels higher than the suggested activation threshold

4.2 Methods

4.2.1 Lagrangian particle tracking method

The CFD method under the Eulerian framework is an excellent tool to analyze averaged flow pattern inside AAAs. However, due to the unsteady nature of the flow, the effect of the instantaneous flow field in AAAs becomes challenging to be analyzed. This unsteadiness is believed to play a role in the activation of platelets that is believed to be responsible for the thrombus accumulation. Furthermore, it can also affect the dynamic of platelets and chemical species responsible for the formation and accumulation of thrombus [9]. Here, the Lagrangian particle tracking method is used to estimate the level of activation of platelets in AAAs and study its relationship with the accumulation of thrombus. Platelets, represented by Lagrangian particles, were tracked by solving the particle equation:

$$\frac{d\boldsymbol{x}^p}{dt} = \boldsymbol{v}^p, \tag{4.1}$$

where $\boldsymbol{x}^p \; and \; \boldsymbol{v}^p$ represent the position and velocity of the particle, respectively. The particles are assumed to be massless and particles' velocities are interpolated from the CFD flow field calculation using shape functions. These particles were seeded every 0.005s (200 release times throughout one cycle) from a plane normal to the centerline at the level of the lower renal branch. Approximately, 3 million particles were released per cardiac cycle, which accounts for 0.1% of the normal platelet concentration in humans (150,000 platelets/mm^3). The number of particle released per time step depended on the volumetric flow rate in order to preserve a uniform concentration at all times.

Each particle was tracked using a parallel in-house code, where an Euler method was used to discretize the particle equation Eq. 4.1 To maintain numerical stability, all

particles were constrained to move a distance of 1/10th of the element's characteristic length that contained them; therefore, each particle time step was independently adapted to meet this criterion. Particles were continuously released until time averaged values of interest (platelet activation potential) did not changed between cardiac cycles. At each time step, the shear stress exerted on each particle was calculated and used for the estimation of the platelet activation potential (PLAP). PLAP was calculated using a power law exposure time model [11]

$$PLAP(\boldsymbol{x};\ \boldsymbol{x}_0^p, t_o^p) = \int_{t_o^p}^{T} [\tau^p(\ \boldsymbol{x}^p(t), t)]^{\ \alpha} dt\ , \tag{4.2}$$

where $\boldsymbol{x}_0^p, t_o^p$, τ^p, $\boldsymbol{x}$, T, and α represent the initial seeding position, initial seeding time, the scalar value of the stress, particle position, time at position $\boldsymbol{x}$, and the power law coefficient constant ($\alpha = 2.28$) chosen to compare values to Hellums locus [45]; respectively. The scalar value of the stress is defined as:

$$\tau^p = \sqrt{2}\mu\|\boldsymbol{D}\|_F \qquad \text{and} \qquad \|\boldsymbol{D}\|_F = \sqrt{tr(\boldsymbol{D}\boldsymbol{D}^T)}\ , \tag{4.3}$$

where $\|\boldsymbol{D}\|_F$ represents the Forbenius norm of the symmetric part of the velocity gradient tensor at the particle position.

$$\|\boldsymbol{D}\|_F = \sqrt{tr(\boldsymbol{D}\boldsymbol{D}^T)} \tag{4.4}$$

While Eq. 4.2 provides an estimation of the activation levels on each seeded platelet at any time, does not provide meaningful information about activation levels on specific near wall regions that experienced ILT accumulation. To enable this analysis, platelet activation levels at near wall regions were extracted from the Lagrangian analysis by dividing the lumen volume (Ω_l) into small control volumes or subdomains ($\Omega_l = \sum_{i=1}^{N_{cell}} \Omega_l^j$) and averaging the contribution of each particle visiting each subdomain over a cardiac cycle:

$$\overline{PLAP}\left(\Omega_l^j\right) = \frac{1}{N_t}\sum_{k=1}^{N_t}\sum_{m\epsilon S}\frac{1}{|S|}PLAP(t_k; x_o^m, t_o^m), \quad (4.5)$$

where Ω_l^j is the subdomain corresponding to the cell used for the CFD flow field calculation, $S\left(\Omega_l^j, t_k\right) = \left\{m|\ x\left(t_k; x_0^p, t_0^p\right)\epsilon\ \Omega_l^j\right\}$ is the set of particles visiting the subdomain Ω_l^j at time t, $|S|$ number of particles visiting Ω_l^j at time t, N_t is the number of time steps per cardiac cycle, and $PLAP(t_k; x_o^m, t_o^m)$ is the platelet activation potential of the platelet "m" from time $t_o$to time t_k. The value of the activation potential associated to each vessel nodal point on the lumen surface was assigned to the one from the subdomain or cell located at a normal distance "d" from the lumen wall (d=0.5 mm).

In addition to the PLAP parameters, a variable called "thrombus formation potential (TFP)" was also estimated and included for the present analysis. This metrics combines the effect of the flow-induced platelet activation with the susceptibility of the endothelium to adhere thrombus [22];

$$TFP(x) = ECAP(x)\overline{PLAP}(x) \quad (4.6)$$

4.3 Results

4.3.1 Local association between PLAP, TFP and local changes in thrombus thickness

Correlation analysis performed to test the local association between regional changes in thrombus thickness and local hemodynamic parameters derived from a Lagrangian particle method such as PLAP and TFP are presented in this chapter (Table 4.1).

PLAP

ID	Scan # 1	2	3	4	5	6
1	-0.39					
2	-0.36	0.14				
3	-0.08					
5	-0.05	0.13	-0.52	-0.37	0.25	
6	-0.03	0.01	0.02	0.02	-0.15	0.08
8	-0.28	0.37	-0.16	-0.28		
9	-0.31	-0.04	-0.23	-0.08		
10	0.07	-0.11	-0.10			
11	-0.26	-0.06	0.18	0.15		
12	-0.37	-0.01	0.25	0.00	0.32	
13	0.04	-0.15	0.07			
14	-0.20	0.11				

TFP

ID	Scan # 1	2	3	4	5	6
1	-0.31					
2	-0.34	0.09				
3	0.02					
5	0.08	0.43	-0.20	-0.06	0.36	
6	-0.01	0.08	0.16	0.07	-0.10	0.04
8	-0.23	0.53	0.25	-0.14		
9	-0.12	0.07	-0.04	0.02		
10	0.26	0.14	0.14			
11	-0.12	-0.19	0.35	-0.12		
12	-0.14	-0.07	0.45	0.00	-0.13	
13	-0.32	-0.08	0.21			
14	0.16	0.06				

Table 4.1 *Correlation between ∆ILT and (a) PLAP, (b) TFP for each scan of each AAA*

Results from the analysis revealed that from all the scans of all AAAs tested, 22.5 and 30% of them showed a direct ∆ILT-PLAP and ∆ILT-TFP relationships, respectively (Figure 4.1a). In both variables, the number of scans showing a weak correlation was approximately the same, but TFP showed larger number of scans with a moderated and strong correlations in comparison to the correlation found with PLAP (Figure 4.1b).

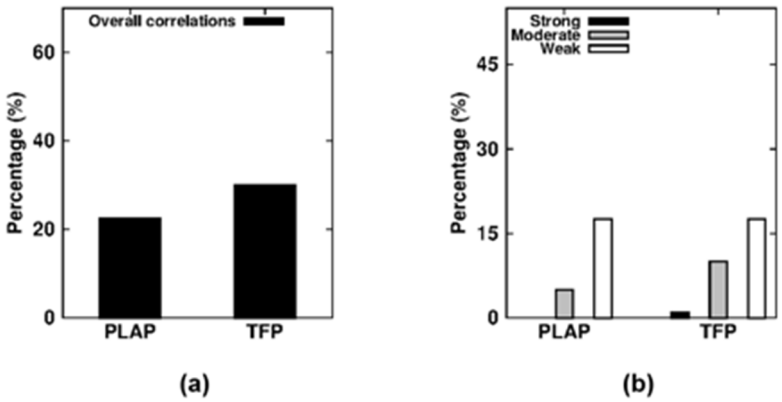

Figure 4.1 *Percentage of number of scans showing an (a) overall and a (b) strong, moderate and weak correlations between ∆ILT and PLAP and TFP.*

Qualitative examination of the spatial distribution of hemodynamic variables such as PLAP and TFP at time point "i" on regions where positives changes in thrombus thickness ($\Delta ILT > 0$) between times i and $i+1$ was performed. This analysis showed some trends in some patients at specific scans. This is the case of P08 at scan 2 that despite regions of high PLAP coincided with regions of ΔILT, high values of TFP were able to clearly depict regions of positive thrombus accumulation in this scan. (Figure 4.2).

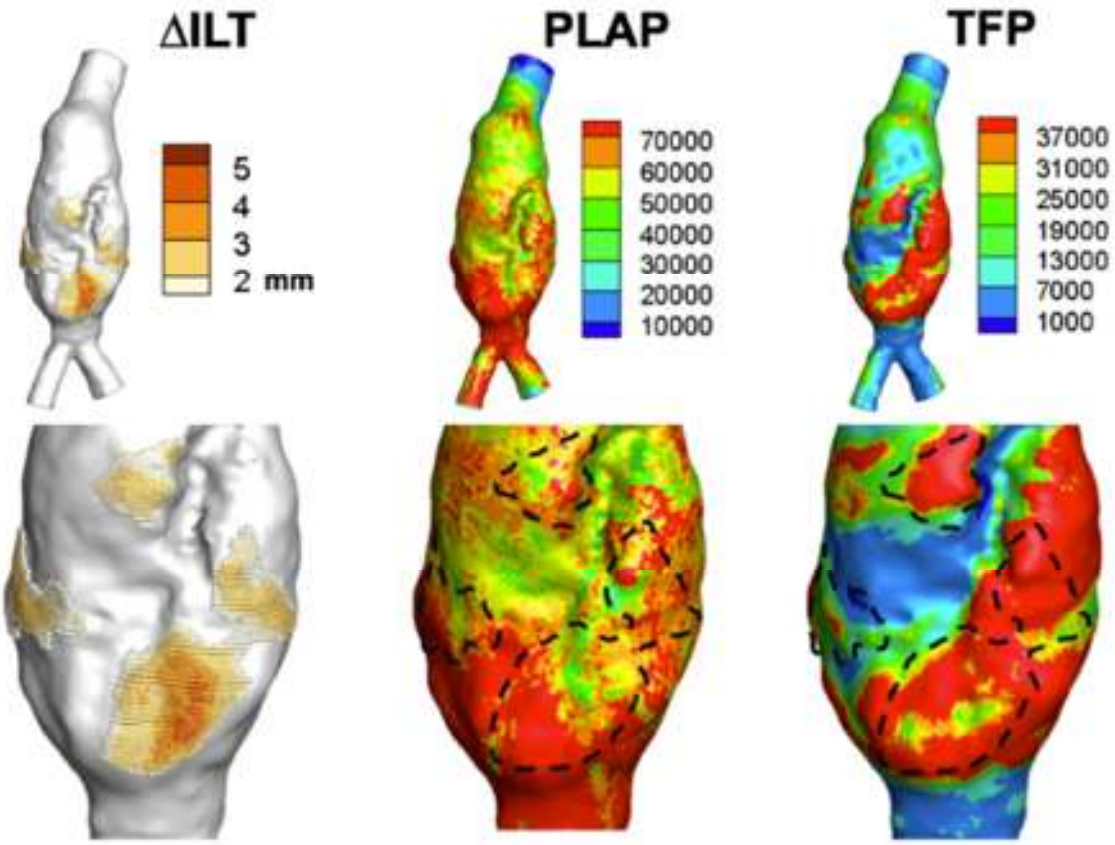

Figure 4.2 *Spatial distribution of ΔILT, PLAP, and TFP for P08 at scan 2 showing that although no specific trend was found in PLAP distribution, high values of TFP coincided with regions of positive ILT thickness changes.*

4.3.2 Platelet activation potential levels

Levels of platelet activation were tested in all AAAs different time point. This cumulative shear rate calculation was performed using a power law model with a coefficient α=2.28. the power low coefficient α was selected in order to compare the estimated activation levels with the locus of activation proposed by Hellums and colleagues [45]. Results of the mean and 95th values of the activation potential recorded in all scan are presented here (Figure 4.3, 4.4).

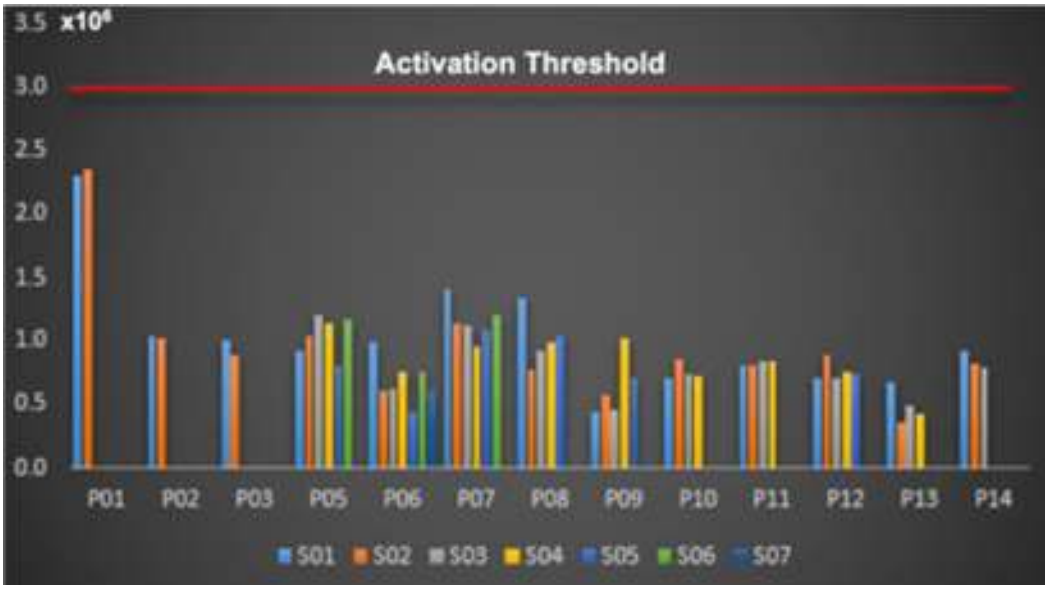

Figure 4.3 *95th percentile values of PLAP for all the scans of all AAAs*

These results showed that none of the AAAs tested at any time-point recorded values close to the threshold activation. The highest activation potential found among all AAAs was recorded in P01. Interestegly, in this AAAs, a very small accumulation of thrombus was seen in comparison to others AAAs that developed thicker thrombus layers (e.g. P09, P13). Also, by comparing average (Figure 4.4) from 95th (Figure 4,3) percentile

it can be seen a large difference between both values, which suggests that platelets inside these AAAs are exposed to large ranges of activation potential.

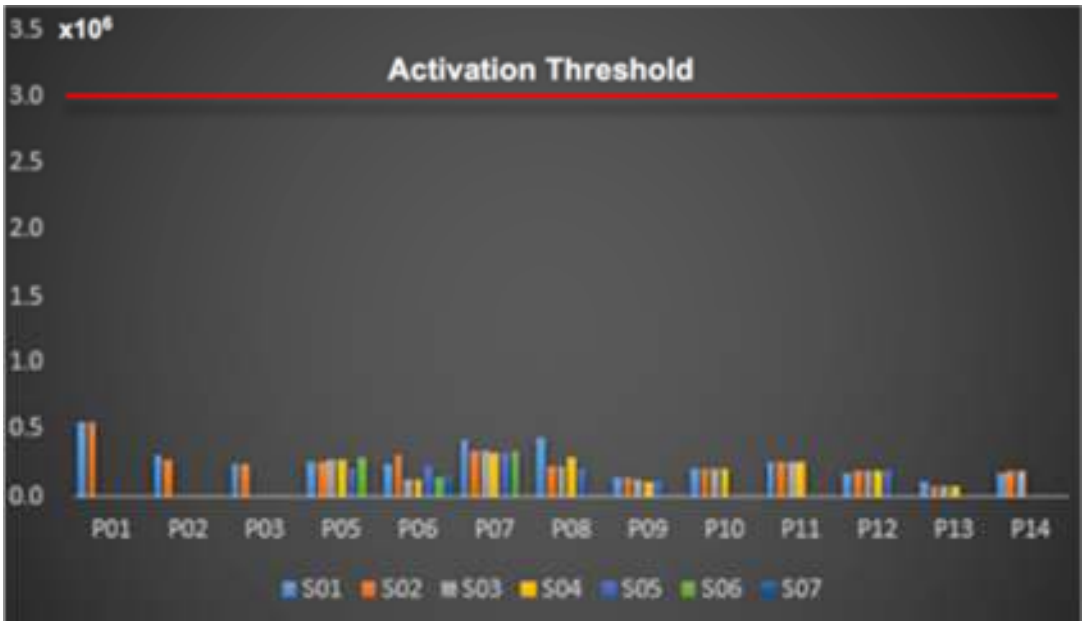

Figure 4.4 *Mean values of PLAP for all the scans of PLAP for all the scans of all AAAs*

4.4 Discussion

The mechanisms leading to the initiation of thrombus were investigated here. Specifically, the theory that suggests that platelet activation is mechanically induced due to the high shear these particles are exposed while being convected to regions suitable for accumulation. The analysis was performed by measuring platelet activation levels in all AAAs at all available time-points (scans) and recording averaged and 99th percentile values of PLAP within the aneurysms. Results from this analysis showed that none of the AAAs reached the suggested activation potential. Also, local hemodynamic parameter measured on the lumen wall (e.g. PLAP and TFP) derived from analysis were also calculated. These values were later correlated to measured changes in thrombus

thickness between two consecutives scans. Results from the analysis showed that just 22.5% and 30.0% of the scans showed an overall correlation between the aforementioned parameters and ΔILT, respectively.

This study used a power law platelet activation model. This model is suggested to better reflect the activation of platelets in comparison to a linear stress-time cumulative model. Here, the exponent (α) was set to 2.28 to allow to compare results with the locus of platelets activation proposed by Hellums and colleagues [45]. Results from measurements showed that 95th percentile values of all AAAs (xx scans) tested here showed that none of them at any time-point reached nor exceeded the activation potential. A recent study also measured this activation potential in 10 small AAAs reaching similar results as the one found in this study [43]. These finding would suggest that mechanically induced platelet activation might not be a kay mechanisms in the formation of thrombus inside AAAs

Despite PLAP values did not reach the activation potential, there was still a possibility that the PLAP variable along or in conjunction with other hemodynamic parameters (e.g. TFP) could be associated to ΔILT. This was tested first using Pearson correlation coefficients and ultimately qualitatively by observing at the spatial distribution of PLAP and TFP on regions where positive ΔILT was observed. Correlation studies, revealed, that among all scans of all AAAs tested, just 22.5 % of them showed weak or moderated correlation between ΔILT and PLAP. Similarly, results from testing the ΔILT-TFP relationship showed that 30.0% showed an overall correlation. For the TFP variable, however, more scans showed a moderated and a strong correlation in comparison to correlations using PLAP.

Qualitatively examination performed to TFP on regions of ILT accumulations, however, showed that in some scans of some AAAs, high values of TFP could predict the accumulation of thrombus (P08 at S02). These findings agree with previous studies that have qualitative associated 90^{th} percentile values of TFP with regions of positive accumulation [22].

It is important to mention that PLAP values were measured at the abdominal level area; specifically, between the renal level and the common iliacs. There is a probability that particles might be exposed to high stresses before entering our area of interest. Although a sensitivity analysis should be performed to estimate this effect, values found in this study were much lower than the suggested activation threshold.

In closing, this chapter tested the hypothesis of a mechanically induced platelet activation as a mechanism responsible of the formation of thrombus inside AAAs [22]. To test the hypothesis, platelet activation levels between the renal level and the common iliac arteries were measured in all AAAs using a Lagrangian particle method. Thus, approximately 3 millions of particles per cardiac cycle, which accounts for about 0.1% of normal platelet concentration in humans were used. On each particle, cumulative activation levels were measured using a power law stress-time model. Results showed that none of particle released in all AAAs reached or exceeded the activation potential. Additionally, the relationship between local changes of thrombus thickness and hemodynamic parameters as PLAP and TFP and results showed that just 22.5 and 30.00% of the scan testes showed an overall correlation. These finding suggests that, although vortical structure might be convecting platelets to regions of activation, platelets are not being activated.

Chapter 5

5.1 Summary of results

Abdominal aortic aneurysms, the permanent focal dilatation of the abdominal aorta [76], is a cardiovascular disease responsible of at least 15.000 deaths. This disease was the 10th leading cause of death within elderly white males in the united states along [3]. Hemodynamics is one of the main contributor to the AAA growth [51] and to the formation of the intraluminal thrombus (ILT) [13]; another important factor that influence the pathogenesis of the disease. Despite the effort to understand the role of each one of these factors to the progression of AAAs, these roles are still poorly understood. This study, used 59 CT scans from a longitudinal CT data set from 14 patients diagnosed with AAA and study the role of hemodynamics in the progression of AAAs and the formation of the intraluminal thrombus.

In chapter 2, we explored this complex relationship by comparing global values of mean TAWSS, AAA expansion and ILT accumulation rates, between AAAs with and without a thrombus accumulation. The amount of ILT accumulation was initially estimated by calculating the spatial distribution of ILT thickness and later measured by using a fraction of lumen area covered by thrombus. The results of this analysis showed that lower values of mean TAWSS and higher values of AAA expansion rates were found in AAAs with ILT in comparisons to those without thrombus. Also, by estimating the spatial distribution of ILT thickness at different time-points, the ILT accumulation process could be described. The ILT showed to initially accumulates on regions of maximum diameter and from there it spread to surrounding regions while thicken on previously covered

regions. Interestedly, this accumulation occurred at the same rate as the AAA expansion rate.

In Chapter 3, we further explored the relationship between hemodynamic and ILT accumulation. Specifically, the relationship between vortical structures, local hemodynamic parameters such as TAWSS, OSI, and ECAP and local changes in thrombus thickness, were qualitative and quantitative studied, respectively. Results of the analysis showed that while AAAs with and without ILT experienced strong vortical structures, vortices on AAAs that experienced ILT consistently dissipated near accumulation regions. Also, by performing a correlation analysis among all local hemodynamic variables measured on the lumen wall, it was found TAWSS showed to be mostly correlated.

Finally, a hypothesis that suggests that mechanically activated platelets might be the leading mechanism promoting thrombus accumulation inside AAA was tested in Chapter 4. Thus, a Lagrangian particle method was used to record shear stress history of a large number of particles (~ 3 millions). In addition, the association between suggested hemodynamic parameters, derived from the particle analysis such as PALP and TFP, and local changes in thrombus thickness was investigated. Results showed that among all scans tested just 22.5% and 30% of them, showed a ΔILT-PLAP and ΔILT-TFP relationship (Figure 4.1a), respectively. Also, by measuring the platelet activation levels it was found that none of the AAAs at any time-point either reached or exceeded the proposed activation potential (Figure 4.3 ,4.4).

The findings presented in this work suggests that ILT formation due to a mechanically induced platelet activation might not be a key mechanism leading to the

formation of thrombus. A recent theory submits the idea that platelets might become activated due to a thromboactive surface. Arguably, thromboactive surfaces form due to abnormal flow patterns and low values of wall shear stress environment that induce endothelium cells (ECs) dysfunction, with impairment of nitric oxide (NO) production [18]. NO has shown to be an effective inhibitor of platelet function [39] and the absent of it on the endothelium would lead to an initial thrombotic event [4]. Our results showed that lower values of wall shear stress were found in AAAs that developed thick ILTs in comparison to those that did not developed thrombus; agreeing with this hypothesis.

Once the initial accumulation occurs, the recruitment and activation of platelets onto thromboactive surfaces can occur at high (> 800 sec-1) and low shear rates (<600sec-1). At high shear rates (> 600-800 sec-1), von Willebrand factor (vwf) plays a critical role due to the strong bonding provided [32]. On the other hand, at low shear rates, the aggregation mechanisms would be highly dependent on fibrinogen biding GPIIb/IIa [40]. Other studies have suggested that platelets would adhere to the AAA lumen surfecs due to the bonding to vWF (at moderate WSS). Shear rates calculated in all AAAs in this study, however, were found be under 600 sec-1 range. At this range, antithrombotic agents have proved to be effective and shear dependent [62]. Our correlation analysis depicted this shear dependency when an inverse correlation between TAWSS and ΔILT was found within regions that experienced thrombus deposition ($\Delta ILT \neq 0$).

However, despite the ΔILT-TAWSS inverse relationship found on such regions, not all zones of low wall shear stress experienced accumulation of thrombus. This suggests that WSS might be an important but not the only factor influencing the accumulation of thrombus. Vortical structures have been suggested to convect platelets and other

chemical species (e.g. Thrombin) to distal regions where thrombus accumulation has been reported [9]. Although our results have shown that ILT accumulation can occur also at proximal regions, the fact vortices on AAAs that developed thrombus consistently dissipated in regions where positive ∆ILT were observed suggest that these coherent structures might be also important in the accumulation of thrombus.

These vortical structure would not just convect platelets to regions of accumulation, but potentially influence the near wall hemodynamic environment [17]. Our results showed this in some AAA that despite their large size, experienced high levels of WSS promoted by a vortical structure swiping the entire lumen surface (P01-S01; Figure 3.6) and this hemodynamic differences could potentially prevent the accumulation of thrombus.

This study also analyzed the role of the ILT accumulation on AAA expansion, which is being debated. Results showed higher AAA expansion rates recorded in AAAs with thick thrombus compared to those that remained without ILT. This results suggests thick ILT layer might be weakening the arterial wall through inducing hypoxia [74], wall thinning, cell inflammation, apoptosis of SMCs, and degradation of the extracellular matrix in walls covered by thick thrombus [49], promoting AAA growth. Interestedly, AAA expansion rate was the same as ILT accumulation rate, suggesting that ILT might be occupying expanded areas, maintaining a nearly constant lumen cross section, which arguably would promote a nearly constant low WSS levels.

In closing, hemodynamic forces are being showed to influence the AAA expansion and ILT accumulation rates. While high WSS values would prevent ILT accumulation, low values of WSS would arguably promote thromboactive surface, which in turn would promote the formation of thrombus. Once these surfaces become thromboactive, the ILT

accumulation would be greatly influenced by vortical structure and local hemodynamic conditions (e.g. WSS). Specifically, Vortical structures would convect platelets and main chemical species (e.g. thrombin) to regions of accumulation, while local hemodynamic variables such as wall shear stress would regulate the platelet recruitment and the formation of thrombus.

The main contribution of this study are the followings:

1. By depicting the ILT thickness distribution at different time-points (scans), the accumulation of thrombus could be described and thus many hypothesis about the location of the initial thrombus deposition and subsequently accumulation were clarified.
2. By comparing AAAs with and without a significant thrombus accumulation, our finding supports the idea of thick ILTs promoting AAA expansion rates.
3. Among all local hemodynamic variables suggested, TAWSS showed to be an important parameter in the accumulation of thrombus.
4. Vortical Structures showed to be a factor in the accumulation of thrombus by convecting platelets and main chemical species (e.g. thombin) on regions suitable for thrombus accumulation.
5. Measuring platelet activation levels, our study found that none of the AAAs studied reached high levels for platelets to activates, suggesting the mechanically induced platelet activation not to be an important mechanism in the accumulation of thrombus.

Some of these findings are being already incorporated in the development of a data-driven approaches for the estimation of the initiation and accumulation of ILT and its effect of AAA expansion. For instance, Farsad et al [28] , incorporated the relationship between AAA expansion and ILT accumulation rates to developed a data-driven growth and remodeling (G&R) formation that included the effect of ILT accumulation. As a future direction, the Cardiovascular Tissue and Mechanics Laboratory will use the findings of this study and develop more enhanced models to integrate hemodynamics into AAA growth (G&R), which enables us to investigate the influence of the hemodynamic environment onto the production of main chemical species for the thrombus formation.

BIBLIOGRAPHY

BIBLIOGRAPHY

1. Adolph, R., D. A. Vorp, D. L. Steed, M. W. Webster, M. V. Kameneva, and S. C. Watkins. Cellular content and permeability of intraluminal thrombus in abdominal aortic aneurysm. *J. Vasc. Surg.* 25:916–926, 1997.

2. Alemu, Y., and D. Bluestein. Flow-induced platelet activation and damage accumulation in a mechanical heart valve: numerical studies. *Artif. Organs* 31:677–688, 2007.

3. Anderson, R. N. Deaths: leading causes for 2000. *Natl. Vital Stat. Rep. Cent. Dis. Control Prev. Natl. Cent. Health Stat. Natl. Vital Stat. Syst.* 50:1–85, 2002.

4. Ando, J., and K. Yamamoto. Effects of Shear Stress and Stretch on Endothelial Function. *Antioxid. Redox Signal.* 15:1389–1403, 2010.

5. Arzani, A., G.-Y. Suh, R. L. Dalman, and S. C. Shadden. A longitudinal comparison of hemodynamics and intraluminal thrombus deposition in abdominal aortic aneurysms. *Am. J. Physiol. - Heart Circ. Physiol.* ajpheart.00461.2014, 2014.doi:10.1152/ajpheart.00461.2014

6. Basciano, C., C. Kleinstreuer, S. Hyun, and E. A. Finol. A relation between near-wall particle-hemodynamics and onset of thrombus formation in abdominal aortic aneurysms. *Ann. Biomed. Eng.* 39:2010–2026, 2011.

7. Biasetti, J., T. C. Gasser, M. Auer, U. Hedin, and F. Labruto. Hemodynamics of the Normal Aorta Compared to Fusiform and Saccular Abdominal Aortic Aneurysms with Emphasis on a Potential Thrombus Formation Mechanism. *Ann. Biomed. Eng.* 38:380–390, 2009.

8. Biasetti, J., F. Hussain, and T. C. Gasser. Blood flow and coherent vortices in the normal and aneurysmatic aortas: a fluid dynamical approach to intra-luminal thrombus formation. *J. R. Soc. Interface R. Soc.* 8:1449–1461, 2011.

9. Biasetti, J., P. G. Spazzini, J. Swedenborg, and T. C. Gasser. An Integrated Fluid-Chemical Model Toward Modeling the Formation of Intra-Luminal Thrombus in Abdominal Aortic Aneurysms. *Front. Physiol.* 3:, 2012.

10. Bluestein, D., K. Dumont, M. De Beule, J. Ricotta, P. Impellizzeri, B. Verhegghe, and P. Verdonck. Intraluminal thrombus and risk of rupture in patient specific abdominal aortic aneurysm - FSI modelling. *Comput. Methods Biomech. Biomed. Engin.* 12:73–81, 2009.

11. Bluestein, D., L. Niu, R. T. Schoephoerster, and M. K. Dewanjee. Fluid mechanics of arterial stenosis: Relationship to the development of mural thrombus. *Ann. Biomed. Eng.* 25:344–356, 1997.

12. Boussel, L., V. Rayz, C. McCulloch, A. Martin, G. Acevedo-Bolton, M. Lawton, R. Higashida, W. S. Smith, W. L. Young, and D. Saloner. Aneurysm growth occurs at region of low wall shear stress: patient-specific correlation of hemodynamics and growth in a longitudinal study. *Stroke* 39:2997, 2008.

13. Boyd, A. J., D. C. S. Kuhn, R. J. Lozowy, and G. P. Kulbisky. Low wall shear stress predominates at sites of abdominal aortic aneurysm rupture. *J. Vasc. Surg.* , 2015.doi:10.1016/j.jvs.2015.01.040

14. Brady, A. R., S. G. Thompson, F. G. Fowkes, R. M. Greenhalgh, and J. T. Powell. Abdominal Aortic Aneurysm Expansion Risk Factors and Time Intervals for Surveillance. *Circulation* 110:16–21, 2004.

15. Brown, C. H., L. B. Leverett, C. W. Lewis, C. P. Alfrey, and J. D. Hellums. Morphological, biochemical, and functional changes in human platelets subjected to shear stress. *J. Lab. Clin. Med.* 86:462–471, 1975.

16. Chatzizisis, Y. S., A. U. Coskun, M. Jonas, E. R. Edelman, C. L. Feldman, and P. H. Stone. Role of Endothelial Shear Stress in the Natural History of Coronary Atherosclerosis and Vascular Remodeling. *J. Am. Coll. Cardiol.* 49:2379–2393, 2007.

17. Chen, C.-Y., R. Antón, M. Hung, P. Menon, E. A. Finol, and K. Pekkan. Effects of Intraluminal Thrombus on Patient-Specific Abdominal Aortic Aneurysm Hemodynamics via Stereoscopic Particle Image Velocity and Computational Fluid Dynamics Modeling. *J. Biomech. Eng.* 136:31001-31001–9, 2014.

18. Chiu, J.-J., and S. Chien. Effects of disturbed flow on vascular endothelium: pathophysiological basis and clinical perspectives. *Physiol. Rev.* 91:327–387, 2011.

19. Cohen, J. CHAPTER 4 - Differences between Correlation Coefficients. In: Statistical Power Analysis for the Behavioral Sciences (Revised Edition). Academic Press, 1977, pp. 109–143.doi:10.1016/B978-0-12-179060-8.50009-8

20. Dalman, R. L. Oxidative stress and abdominal aneurysms: how aortic hemodynamic conditions may influence AAA disease. *Cardiovasc. Surg. Lond. Engl.* 11:417–419, 2003.

21. Darling, R. C., C. R. Messina, D. C. Brewster, and L. W. Ottinger. Autopsy study of unoperated abdominal aortic aneurysms. The case for early resection. *Circulation* 56:II161-164, 1977.

22. Di Achille, P., G. Tellides, C. A. Figueroa, and J. D. Humphrey. A haemodynamic predictor of intraluminal thrombus formation in abdominal aortic aneurysms. *Proc. R. Soc. Lond. Math. Phys. Eng. Sci.* 470:20140163, 2014.

23. Di Achille, P., G. Tellides, and J. D. Humphrey. Hemodynamics-driven deposition of intraluminal thrombus in abdominal aortic aneurysms. *Int. J. Numer. Methods Biomed. Eng.* 33:n/a-n/a, 2017.

24. Di Martino, E. S., A. Bohra, J. P. Vande Geest, N. Gupta, M. S. Makaroun, and D. A. Vorp. Biomechanical properties of ruptured versus electively repaired abdominal aortic aneurysm wall tissue. *J. Vasc. Surg.* 43:570–576, 2006.

25. Di Martino, E. S., S. Mantero, F. Inzoli, G. Melissano, D. Astore, R. Chiesa, and R. Fumero. Biomechanics of abdominal aortic aneurysm in the presence of endoluminal thrombus: Experimental characterisation and structural static computational analysis. *Eur. J. Vasc. Endovasc. Surg.* 15:290–299, 1998.

26. Doyle, B. J., T. M. McGloughlin, E. G. Kavanagh, and P. R. Hoskins. From Detection to Rupture: A Serial Computational Fluid Dynamics Case Study of a Rapidly Expanding, Patient-Specific, Ruptured Abdominal Aortic Aneurysm. In: Computational Biomechanics for Medicine, edited by B. Doyle, K. Miller, A. Wittek, and P. M. F. Nielsen. Springer New York, 2014, pp. 53–68.

27. Dua, M. M., and R. L. Dalman. Hemodynamic Influences on Abdominal Aortic Aneurysm Disease: Application of Biomechanics to Aneurysm Pathophysiology. *Vascul. Pharmacol.* 53:11–21, 2010.

28. Farsad, M., B. A. Zambrano, and S. Baek. Data-Guided Growth and Remodeling Model of Abdominal Aortic Aneurysm Accounting for the Bio-chemical Effects of Intraluminal Thrombus. In: Computational Biomechanics for Medicine, edited by B. Doyle, K. Miller, A. Wittek, and P. M. F. Nielsen. Springer International Publishing, 2015, pp. 13–23.

29. Finol, E. A., and C. H. Amon. Flow-induced wall shear stress in abdominal aortic aneurysms: Part I--steady flow hemodynamics. *Comput. Methods Biomech. Biomed. Engin.* 5:309–318, 2002.

30. Finol, E. A., and C. H. Amon. Flow-induced wall shear stress in abdominal aortic aneurysms: Part II--pulsatile flow hemodynamics. *Comput. Methods Biomech. Biomed. Engin.* 5:319–328, 2002.

31. Folkesson, M., A. Silveira, P. Eriksson, and J. Swedenborg. Protease activity in the multi-layered intra-luminal thrombus of abdominal aortic aneurysms. *Atherosclerosis* 218:294–299, 2011.

32. Furie, B., and B. C. Furie. In vivo thrombus formation. *J. Thromb. Haemost.* 5:12–17, 2007.

33. Gaillard, E., P. Bergeron, and V. Deplano. Influence of Wall Compliance on Hemodynamics in Models of Abdominal Aortic Aneurysm. *J. Endovasc. Ther.* 14:593–599, 2007.

34. Georgakarakos, E., C. V. Ioannou, S. Volanis, Y. Papaharilaou, J. Ekaterinaris, and A. N. Katsamouris. The influence of intraluminal thrombus on abdominal aortic aneurysm wall stress. *Int. Angiol. J. Int. Union Angiol.* 28:325–333, 2009.

35. Gharahi, H., B. A. Zambrano, C. Lim, J. Choi, W. Lee, and S. Baek. On growth measurements of abdominal aortic aneurysms using maximally inscribed spheres. *Med. Eng. Phys.* , 2015.doi:10.1016/j.medengphy.2015.04.011.

36. Gijsen, F. J. H., F. N. van de Vosse, and J. D. Janssen. Wall shear stress in backward-facing step flow of a red blood cell suspension. *Biorheology* 35:263–279, 1998.

37. Gijsen, F. J., F. N. van de Vosse, and J. D. Janssen. The influence of the non-Newtonian properties of blood on the flow in large arteries: steady flow in a carotid bifurcation model. *J. Biomech.* 32:601–608, 1999.

38. Gimbrone, M. A., K. R. Anderson, and J. N. T. et al. Special communication: the critical role of mechanical forces in blood vessel development, physiology and pathology. *J. Vasc. Surg.* 29:1104–1151, 1999.

39. Gkaliagkousi, E., J. Ritter, and A. Ferro. Platelet-derived nitric oxide signaling and regulation. *Circ. Res.* 101:654–662, 2007.

40. Goto, S., Y. Ikeda, E. Saldívar, and Z. M. Ruggeri. Distinct mechanisms of platelet aggregation as a consequence of different shearing flow conditions. *J. Clin. Invest.* 101:479–486, 1998.

41. Grigioni, M., C. Daniele, U. Morbiducci, G. D'Avenio, G. Di Benedetto, and V. Barbaro. The power-law mathematical model for blood damage prediction: analytical developments and physical inconsistencies. *Artif. Organs* 28:467–475, 2004.

42. Hans, S. S., O. Jareunpoon, M. Balasubramaniam, and G. B. Zelenock. Size and location of thrombus in intact and ruptured abdominal aortic aneurysms. *J. Vasc. Surg.* 41:584–588, 2005.

43. Hansen, K. B., A. Arzani, and S. C. Shadden. Mechanical Platelet Activation Potential in Abdominal Aortic Aneurysms. *J. Biomech. Eng.* 137:041005–041005, 2015.

44. Harter, L. P., B. H. Gross, P. W. Callen, and R. A. Barth. Ultrasonic evaluation of abdominal aortic thrombus. *J. Ultrasound Med. Off. J. Am. Inst. Ultrasound Med.* 1:315–318, 1982.

45. Hellums, J. D. 1993 Whitaker lecture: Biorheology in thrombosis research. *Ann. Biomed. Eng.* 22:445–455, 1994.

46. Humphrey, J. D. Vascular adaptation and mechanical homeostasis at tissue, cellular, and sub-cellular levels. *Cell Biochem Biophys* 50:53–78, 2008.

47. Jang, I. K., H. K. Gold, A. A. Ziskind, J. T. Fallon, R. E. Holt, R. C. Leinbach, J. W. May, and D. Collen. Differential sensitivity of erythrocyte-rich and platelet-rich arterial thrombi to lysis with recombinant tissue-type plasminogen activator. A possible explanation for resistance to coronary thrombolysis. *Circulation* 79:920–928, 1989.

48. Jeong, J., and F. Hussain. On the identification of a vortex. *J. Fluid Mech.* 285:69–94, 1995.

49. Kazi, M., J. Thyberg, P. Religa, J. Roy, P. Eriksson, U. Hedin, and J. Swedenborg. Influence of intraluminal thrombus on structural and cellular composition of abdominal aortic aneurysm wall. *J. Vasc. Surg. Off. Publ. Soc. Vasc. Surg. Int. Soc. Cardiovasc. Surg. North Am. Chapter* 38:1283–1292, 2003.

50. Komorowicz, E., K. Kolev, I. Léránt, and R. Machovich. Flow rate-modulated dissolution of fibrin with clot-embedded and circulating proteases. *Circ. Res.* 82:1102–1108, 1998.

51. Les, A. S., S. C. Shadden, C. A. Figueroa, J. M. Park, M. M. Tedesco, R. J. Herfkens, R. L. Dalman, and C. A. Taylor. Quantification of hemodynamics in abdominal aortic aneurysms during rest and exercise using magnetic resonance imaging and computational fluid dynamics. *Ann. Biomed. Eng.* 38:1288–1313, 2010.

52. Li, Z.-Y., J. U-King-Im, T. Y. Tang, E. Soh, T. C. See, and J. H. Gillard. Impact of calcification and intraluminal thrombus on the computed wall stresses of abdominal aortic aneurysm. *J. Vasc. Surg.* 47:928–935, 2008.

53. Malek, A. M., S. L. Alper, and S. Izumo. Hemodynamic shear stress and its role in atherosclerosis. *JAMA* 282:2035–2042, 1999.

54. Mower, W. R., W. J. Quiñones, and S. S. Gambhir. Effect of intraluminal thrombus on abdominal aortic aneurysm wall stress. *J. Vasc. Surg. Off. Publ. Soc. Vasc. Surg. Int. Soc. Cardiovasc. Surg. North Am. Chapter* 26:602–608, 1997.

55. Nakahashi, T. K., K. Hoshina, P. S. Tsao, E. Sho, M. Sho, J. K. Karwowski, C. Yeh, R.-B. Yang, J. N. Topper, and R. L. Dalman. Flow Loading Induces Macrophage

Antioxidative Gene Expression in Experimental Aneurysms. *Arterioscler. Thromb. Vasc. Biol.* 22:2017–2022, 2002.

56. Nobili, M., J. Sheriff, U. Morbiducci, A. Redaelli, and D. Bluestein. Platelet Activation Due to Hemodynamic Shear Stresses: Damage Accumulation Model and Comparison to In Vitro Measurements. *ASAIO J. Am. Soc. Artif. Intern. Organs 1992* 54:64–72, 2008.

57. Olufsen, M. S., C. S. Peskin, W. Y. Kim, E. M. Pedersen, A. Nadim, and J. Larsen. Numerical simulation and experimental validation of blood flow in arteries with structured-tree outflow conditions. *Ann. Biomed. Eng.* 28:1281–1299, 2000.

58. Participants, U. S. A. T. Long-term outcomes of immediate repair compared with surveillance of small abdominal aortic aneurysms. *N Engl J Med* 346:1445–1452, 2002.

59. Raghavan, M. L., J. Kratzberg, E. M. Castro de Tolosa, M. M. Hanaoka, P. Walker, and E. S. da Silva. Regional distribution of wall thickness and failure properties of human abdominal aortic aneurysm. *J. Biomech.* 39:3010–3016, 2006.

60. Raghavan, M. L., D. A. Vorp, M. P. Federle, M. S. Makaroun, and M. W. Webster. Wall stress distribution on three-dimensionally reconstructed models of human abdominal aortic aneurysm. *J. Vasc. Surg.* 31:760–769, 2000.

61. Ramstack, J. M., L. Zuckerman, and L. F. Mockros. Shear-induced activation of platelets. *J. Biomech.* 12:113–125, 1979.

62. Sakariassen, K. S., L. Orning, and V. T. Turitto. The impact of blood shear rate on arterial thrombus formation. *Future Sci. OA* 1–9, 2015.doi:10.4155/fso.15.28.

63. Salsac, A. V., S. R. Sparks, J. M. Chomaz, and J. C. Lasheras. Evolution of the wall shear stresses during the progressive enlargement of symmetric abdominal aortic aneurysms. *J. Fluid Mech.* 560:19–51, 2006.

64. Schurink, G. W., J. M. van Baalen, M. J. Visser, and J. H. van Bockel. Thrombus within an aortic aneurysm does not reduce pressure on the aneurysmal wall. *J. Vasc. Surg.* 31:501–506, 2000.

65. Shadden, S. C., and S. Hendabadi. Potential fluid mechanic pathways of platelet activation. *Biomech. Model. Mechanobiol.* 12:467–474, 2013.

66. Sheidaei, A., S. C. Hunley, S. Zeinali-Davarani, L. G. Raguin, and S. Baek. Simulation of abdominal aortic aneurysm growth with updating hemodynamic loads using a realistic geometry. *Med. Eng. Phys.* 33:80–88, 2011.

67. Shindo, S., H. Matsumoto, K. Kubota, A. Kojima, M. Matsumoto, K. Satoh, and Y. Ozaki. Is the Size of an Abdominal Aortic Aneurysm Associated with Coagulopathy? *World J. Surg.* 29:925–929, 2005.

68. Shum, J., E. S. DiMartino, A. Goldhamme, D. H. Goldman, L. C. Acker, G. Patel, J. H. Ng, G. Martufi, and E. A. Finol. Semiautomatic vessel wall detection and quantification of wall thickness in computed tomography images of human abdominal aortic aneurysms. *Med. Phys.* 37:638–648, 2010.

69. Sutera, S. P., and M. H. Mehrjardi. Deformation and fragmentation of human red blood cells in turbulent shear flow. *Biophys. J.* 15:1–10, 1975.

70. Swedenborg, J., and P. Eriksson. The intraluminal thrombus as a source of proteolytic activity. *Ann. N. Y. Acad. Sci.* 1085:133–138, 2006.

71. Taylor, C. A., T. J. R. Hughes, and C. K. Zarins. Effect of exercise on hemodynamic conditions in the abdominal aorta. *J. Vasc. Surg.* 29:1077–1089, 1999.

72. Thubrikar, M. J., F. Robicsek, M. Labrosse, V. Chervenkoff, and B. L. Fowler. Effect of thrombus on abdominal aortic aneurysm wall dilation and stress. *J. Cardiovasc. Surg. (Torino)* 44:67–77, 2003.

73. Vardulaki, K. A., T. C. Prevost, N. M. Walker, N. E. Day, A. B. Wilmink, C. R. Quick, H. A. Ashton, and R. A. Scott. Growth rates and risk of rupture of abdominal aortic aneurysms. *Br. J. Surg.* 85:1674–1680, 1998.

74. Vorp, D. A., W. J. Federspiel, and M. W. Webster. Does laminated intraluminal thrombus within abdominal aortic aneurysm cause anoxia of the aortic wall? *J. Vasc. Surg. Off. Publ. Soc. Vasc. Surg. Int. Soc. Cardiovasc. Surg. North Am. Chapter* 23:540–541, 1996.

75. Vorp, D. A., P. C. Lee, D. H. Wang, M. S. Makaroun, E. M. Nemoto, S. Ogawa, and M. W. Webster. Association of intraluminal thrombus in abdominal aortic aneurysm with local hypoxia and wall weakening. *J. Vasc. Surg.* 34:291–299, 2001.

76. Vorp, D. A., W. A. Mandarino, M. W. Webster, and J. Gorcsan III. Potential influence of intraluminal thrombus on abdominal aortic aneurysm as assessed by a new non-invasive method. *Cardiovasc. Surg.* 4:732–739, 1996.

77. Wang, D. H., M. S. Makaroun, M. W. Webster, and D. A. Vorp. Effect of intraluminal thrombus on wall stress in patient-specific models of abdominal aortic aneurysm. *J. Vasc. Surg.* 36:598–604, 2002.

78. Wilson, J. S., L. Virag, P. Di Achille, I. Karsaj, and J. D. Humphrey. Biochemomechanics of intraluminal thrombus in abdominal aortic aneurysms. *J. Biomech. Eng.* 135:21011, 2013.

79. Wood, N. B. Aspects of fluid dynamics applied to the larger arteries. *J. Theor. Biol.* 199:137–161, 1999.

80. Wurzinger, L. J., R. Opitz, P. Blasberg, and H. Schmid-Schönbein. Platelet and coagulation parameters following millisecond exposure to laminar shear stress. *Thromb. Haemost.* 54:381–386, 1985.

81. Yu, S. C. M. Steady and pulsatile flow studies in Abdominal Aortic Aneurysm models using Particle Image Velocimetry. *Int. J. Heat Fluid Flow* 21:74–83, 2000.

82. Zambrano, B. A., H. Gharahi, C. Lim, F. A. Jaberi, J. Choi, W. Lee, and S. Baek. Association of Intraluminal Thrombus, Hemodynamic Forces, and Abdominal Aortic Aneurysm Expansion Using Longitudinal CT Images. *Ann. Biomed. Eng.* , 2015.doi:10.1007/s10439-015-1461-x.